

BO-PBK: A comprehensive solver for dispersion relations of obliquely propagating waves in magnetized multi-species plasma with anisotropic loss-cone drift product-bi-kappa distribution

Wei Bai^a, Huasheng Xie^{b,c}

^a*College of Electrical and Power Engineering, Taiyuan University of Technology, Taiyuan, 030024, China*

^b*Hebei Key Laboratory of Compact Fusion, Langfang, 065001, China*

^c*ENN Science and Technology Development Co., Ltd., Langfang, 065001, China*

Abstract

We present BO-PBK (BO-Product-Bi-Kappa), a new solver for kinetic dispersion relations of obliquely propagating waves in magnetized plasmas with complex velocity distributions. It reformulates the linearized VlasovMaxwell system into a compact eigenvalue problem, enabling direct computation of multiple wave branches and unstable modes without iterative initial-value searches. Key innovations include a unified framework supporting product-bi-kappa, kappa-Maxwellian, bi-Maxwellian, and hybrid distributions with multi-component and loss-cone features; a concise rational-form eigenvalue formulation; and a 2-3 times reduction in matrix dimensions compared to the BO-KM solver, with improved efficiency at larger kappa indices. Benchmark tests confirm accurate reproduction of standard kinetic results and efficient resolution of waves and instabilities. BO-PBK thus provides a computationally efficient tool for wave and stability analysis in space and laboratory plasmas.

Keywords: Product-bi-kappa distribution, Kinetic dispersion relation, Waves and instabilities, Eigenvalue problem

Email addresses: baiwei12@mail.ustc.edu.cn, baiweiphys@gmail.com (Wei Bai), xiehuasheng@enn.cn, huashengxie@gmail.com (Huasheng Xie)

1. Introduction

In laboratory and space plasmas, superthermal particles often follow non-Maxwellian distributions, which are well described by the family of Kappa distributions [1, 2, 3]. These distributions exhibit Maxwellian-like behavior at low energies and a power-law decay at high energies, yielding a high-energy tail substantially broader than that of an exponential decay [4, 5]. The modified plasma dispersion function for kappa distributions, introduced by Summers and Thorne [6, 7], is essential for analyzing kinetic plasma instabilities, especially in systems with complex distributions such as the bi-kappa (BK) [6], product-bi-kappa (PBK) [8, 6, 9], and subtracted-kappa (SK)[10] distributions. Mace and Hellberg [11] further generalized this dispersion function by allowing the κ index to take any positive real value greater than 3/2. For solar wind ion and electron data from IMP detection[8], the PBK distribution may provide a better or at least comparable fit than bi-Maxwellian (BM) or BK distributions [2]. By decoupling the parallel and perpendicular dynamics of plasma particles respect to the magnetic field [1], the PBK model enables flexible representation of temperature anisotropy, with independent definitions of parallel temperature T_{\parallel} , perpendicular temperature T_{\perp} , and corresponding parameters κ_{\parallel} and κ_{\perp} . In the limit $\kappa_{\perp} \rightarrow \infty$, the PBK reduces to the kappa-Maxwellian (KM) distribution form [12, 13, 14, 15]; when both $\kappa_{\parallel}, \kappa_{\perp} \rightarrow \infty$, it converges to the BM distribution [9].

Numerous solvers based on linearized Vlasov-Maxwell equations have been developed for Maxwellian and non-Maxwellian plasmas [3] . These include solvers for BM (e.g., WHAMP [16], PLADAWAN [17], PLUME [18], NHDS [19], PDRK [20], BO [21]), BK (e.g., DHSARK [22], DIS-K [23], parallel drift BK [24]), KM (e.g., BO-KM [15], KUPDAP [25]), and arbitrary distributions (e.g., LEOPARD [26], ALPS [27, 28], BO-Arbitrary [29]). Listed in Table 1, the BO-family solvers employ a matrix method to model plasmas with various distributions (BM, KM, PBK, and arbitrary gyrotrropic, incorporating parallel, perpendicular drift, ring-beam, and loss-cone features). The BO-Arbitrary code [29] expands the distribution function using Hermite basis functions and transforms the dispersion relation into a matrix eigenvalue problem via rational approximation, though its fitting accuracy for low-order kappa distributions is limited.

Building on these advances, this paper presents the BO-PBK solver, a new eigenvalue-based approach for analyzing waves and instabilities of obliquely propagating waves in magnetized multi-component plasmas. The solver sup-

ports drifting distributions (PBK, KM, BM), and their loss-cone hybrids. The method reformulates the generalized dielectric tensor for such plasmas as a linear eigenvalue system. This reformulation eliminates the need for initial-value iteration and enables the accurate, one-time calculation of all significant eigenroots. Furthermore, this paper elaborates on the eigenvalue system construction of the solver and presents numerical verification.

Table 1: List of BO-family solvers

Solver	PDRK [20]	BO [21]	BO-Arbitray [29]	BO-KM [15]	BO-PBK
Distribution	BM (Drift)	BM (Loss-cone, Drift, Ring beam)	Arbitrary	KM/BM (Drift)	PBK/KM/BM (Loss-cone, Drift)

KM/BM: KM, BM, and their multi-component mixed-distribution plasmas; PBK/KM/BM: PBK, KM, BM, and their multi-component mixed-distribution plasmas.

This paper is organized as follows. Section 2 introduces the models of PBK-Maxwellian plasma distribution models and derives the concise dispersion tensors. Section 3 details the construction of the eigenvalue system for the solver. Section 4 presents benchmark studies for the new solver. Finally, Section 5 concludes and discusses the findings.

2. Hybrid kinetic model for PBK-Maxwellian plasmas

Based on the Vlasov-Maxwell equations, we derive a concise rational expression for the susceptibility tensor of a PBK plasma. This formulation reduces to the well-established rational forms of KM and BM susceptibility tensors in the Maxwellian limit, thereby providing a unified description across these distribution models.

2.1. PBK plasma distribution functions

This study considers plasma particles governed by loss-cone drift PBK distributions with direction-dependent indices $\kappa_{\parallel s}$ and $\kappa_{\perp s}$ for the s th species,

given by

$$\begin{cases} f_{s0}(v_{\parallel}, v_{\perp}) = f_{s0}^{\text{PBK}}(v_{\parallel}, v_{\perp}^2) = f_{s\parallel}^{\text{K}}(v_{\parallel}) f_{s\perp}^{\text{K}}(v_{\perp}^2), \\ f_{s\parallel}^{\text{K}}(v_{\parallel}) = \frac{1}{\sqrt{\pi}\theta_{\parallel s}} \frac{\Gamma(\kappa_{\parallel s}+1)}{\sqrt{\kappa_{\parallel s}}\Gamma(\kappa_{\parallel s}+1/2)} \left[1 + \frac{(v_{\parallel}-u_{s0})^2}{\kappa_{\parallel s}\theta_{\parallel s}^2}\right]^{-(\kappa_{\parallel s}+1)}, \\ f_{s\perp}^{\text{K}}(v_{\perp}^2) = \frac{1}{\pi\theta_{\perp s}^2\kappa_{\perp s}^{\sigma_s+1}} \frac{\Gamma(\kappa_{\perp s}+\sigma_s+1)}{\Gamma(\sigma_s+1)\Gamma(\kappa_{\perp s})} \left(\frac{v_{\perp}}{\theta_{\perp s}}\right)^{2\sigma_s} \left(1 + \frac{v_{\perp}^2}{\kappa_{\perp s}\theta_{\perp s}^2}\right)^{-(\kappa_{\perp s}+\sigma_s+1)}, \end{cases} \quad (1)$$

in polar coordinates $(v_x, v_y, v_z) = (v_{\perp} \cos \phi, v_{\perp} \sin \phi, v_{\parallel})$ of the particle velocity space, where v_{\parallel} and v_{\perp} are the velocity components parallel and perpendicular to the background magnetic field \mathbf{B}_0 , respectively. The PBK distribution is normalized to unity, i.e., $\int f_{s0} d^3v = 1$. The parallel and perpendicular thermal velocities, $\theta_{\parallel s}$ and $\theta_{\perp s}$, are defined by

$$\theta_{\parallel s} = \left[\frac{(2 - 1/\kappa_{\parallel s})k_B T_{\parallel s}}{m_s} \right]^{1/2}, \quad \theta_{\perp s} = \left[\frac{2(1 - 1/\kappa_{\perp s})k_B T_{\perp s}}{m_s(\sigma_s + 1)} \right]^{1/2}, \quad (2)$$

with the indices constrained by $\kappa_{\parallel s} > 1/2$ and $\kappa_{\perp s} > 1$, respectively. Here k_B is Boltzmann's constant and m_s denotes particle mass, and the field-aligned drift velocity is $u_{s0} = \int_{-\infty}^{\infty} f_{s\parallel}^{\text{K}} v_{\parallel} dv_{\parallel}$. The PBK distribution used here (Eqs. (1)) has an exponent differing by one from that in Ref. [9], which results in a corresponding unit offset in the kappa index of the dispersion relation, as confirmed by both analytical and numerical results.

In Maxwellian limit ($\kappa_{\perp s} \rightarrow \infty$), the loss-cone drift PBK distribution (1) transforms into the loss-cone drift KM distribution function, given by

$$f_{s0}^{\text{KM}}(v_{\parallel}, v_{\perp}^2) = \lim_{\kappa_{\perp s} \rightarrow \infty} f_{s0}^{\text{PBK}}(v_{\parallel}, v_{\perp}^2) = f_{s\parallel}^{\text{K}}(v_{\parallel}) f_{s\perp}^{\text{M}}(v_{\perp}^2). \quad (3)$$

Furthermore, when the loss-cone drift PBK distribution (1) is in Maxwellian limits ($\kappa_{\parallel s} \rightarrow \infty$ and $\kappa_{\perp s} \rightarrow \infty$), it takes the form of the loss-cone drift BM distribution, denoted as

$$f_{s0}^{\text{BM}}(v_{\parallel}, v_{\perp}^2) = \lim_{\kappa_{\parallel s}, \kappa_{\perp s} \rightarrow \infty} f_{s0}^{\text{PBK}}(v_{\parallel}, v_{\perp}^2) = f_{s\parallel}^{\text{M}}(v_{\parallel}) f_{s\perp}^{\text{M}}(v_{\perp}^2). \quad (4)$$

Here, $f_{s\parallel}^{\text{M}}$ and $f_{s\perp}^{\text{M}}$ represent the Maxwellian distribution functions for velocity components parallel and perpendicular to the magnetic field, respectively. They can be expressed as follows,

$$\begin{cases} f_{s\parallel}^{\text{M}}(v_{\parallel}) = \lim_{\kappa_{\parallel s} \rightarrow \infty} f_{s\parallel}^{\text{K}}(v_{\parallel}) = \frac{1}{\sqrt{\pi}\theta_{\parallel s}} \exp \left[-\frac{(v_{\parallel}-u_{s0})^2}{\theta_{\parallel s}^2} \right], \\ f_{s\perp}^{\text{M}}(v_{\perp}^2) = \lim_{\kappa_{\perp s} \rightarrow \infty} f_{s\perp}^{\text{K}}(v_{\perp}^2) = \frac{1}{\pi\theta_{\perp s}^2\Gamma(\sigma_s+1)} \left(\frac{v_{\perp}}{\theta_{\perp s}}\right)^{2\sigma_s} \exp \left(-\frac{v_{\perp}^2}{\theta_{\perp s}^2} \right), \end{cases} \quad (5)$$

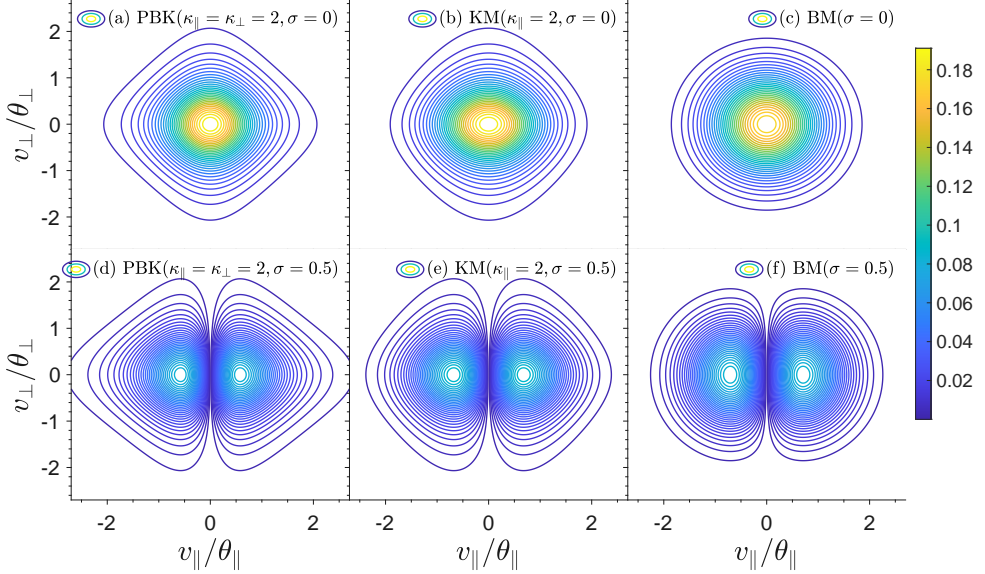


Figure 1: Contours of the normalized electron velocity distribution functions in the $(v_{\parallel}, v_{\perp})$ plane with $T_{\parallel e} = T_{\perp e} = 1 \times 10^2$ eV. Panels (a)-(c) show the PBK, KM, and BM distributions without a loss-cone, while panels (d)-(f) show the corresponding distributions with a loss-cone $\sigma = 0.5$.

where $\tilde{\theta}_{\parallel s}$ and $\tilde{\theta}_{\perp s}$ denote the thermal speeds parallel and perpendicular to the magnetic field in Maxwellian plasma, respectively, and are defined as:

$$\tilde{\theta}_{\parallel s} = \left(\frac{2k_B T_{\parallel s}}{m_s} \right)^{1/2}, \quad \tilde{\theta}_{\perp s} = \left[\frac{2k_B T_{\perp s}}{m_s (\sigma_s + 1)} \right]^{1/2}. \quad (6)$$

Figure 1 shows the contour of normalized electron velocity distributions in the $(v_{\parallel}, v_{\perp})$ planes. Panels (a)-(c) correspond to the PBK, KM, and BM models without a loss-cone, while panels (d)-(f) show the same models with a loss-cone ($\sigma = 0.5$). Figure 2 plots the normalized parallel distributions $f_{\parallel}^K(v_{\parallel})$ and $f_{\parallel}^M(v_{\parallel})$ (left), and the perpendicular distributions $f_{\perp}^K(v_{\perp})$ and $f_{\perp}^M(v_{\perp})$ with $\sigma = 0.5$ (right), revealing that the distribution functions converge toward the Maxwellian distribution with increasing κ_{\parallel} and κ_{\perp} , and are close to it at $\kappa_{\parallel} = \kappa_{\perp} = 200$.

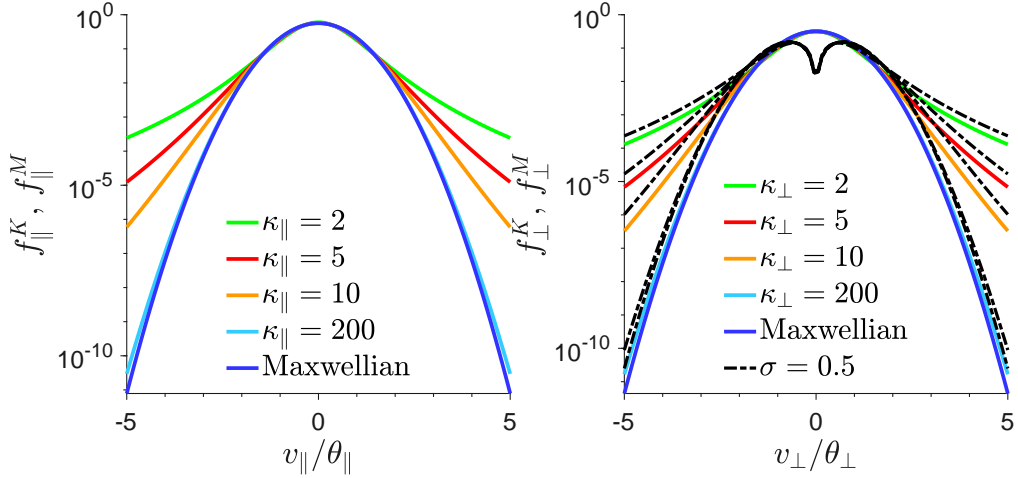


Figure 2: Normalized electron velocity distribution functions for Kappa and Maxwellian models at $T_{\parallel e} = T_{\perp e} = 1 \times 10^2$ eV. Left: parallel distributions $f_{\parallel}^K(v_{\parallel})$ and $f_{\parallel}^M(v_{\parallel})$; right: perpendicular distributions $f_{\perp}^K(v_{\perp})$ and $f_{\perp}^M(v_{\perp})$ with a loss-cone at $\sigma = 0.5$.

2.2. The dispersion tensor for PBK plasma

We consider an obliquely propagating plasma wave ($\propto \exp[i(\mathbf{k} \cdot \mathbf{r} - \omega t)]$), where the wavevector $\mathbf{k} = (k_x, 0, k_z) = (k \sin \theta, 0, k \cos \theta)$ forms an angle θ with the background magnetic field $\mathbf{B}_0 = B_0 \mathbf{e}_z$. The susceptibility tensor $\boldsymbol{\chi}_s$ for a magnetized plasma, derived from the Vlasov-Maxwell equations, contributes to the dielectric tensor as $\boldsymbol{\epsilon}(\boldsymbol{\omega}, \mathbf{k}) = \mathbf{I} + \sum_s \boldsymbol{\chi}_s$, where \mathbf{I} is the unit dyadic and the sum is over all plasma species. The full susceptibility $\boldsymbol{\chi} = \sum_s \boldsymbol{\chi}_s$ is [30, 7, 31],

$$\boldsymbol{\chi} = \sum_s \sum_{n=-\infty}^{\infty} \frac{\omega_{ps}^2}{\omega} \int \frac{v_{\perp} d\mathbf{v}}{\omega - k_{\parallel} v_{\parallel} - n\omega_{cs}} \times \begin{bmatrix} A_s \frac{n^2}{\mu_s^2} J_n^2 & i A_s \frac{n}{\mu_s} J_n J'_n & B_s \frac{n}{\mu_s} J_n^2 \\ -i A_s \frac{n}{\mu_s} J_n J'_n & A_s J_n'^2 & -i B_s J_n J'_n \\ A_s \frac{n}{\mu_s} \frac{v_{\parallel}}{v_{\perp}} J_n^2 & i A_s \frac{v_{\parallel}}{v_{\perp}} J_n J'_n & B_s \frac{v_{\parallel}}{v_{\perp}} J_n^2 \end{bmatrix}, \quad (7)$$

where the velocity-space integral is $\int (\dots) d\mathbf{v} = \int_{-\infty}^{\infty} (\dots) dv_{\parallel} \int_0^{\infty} 2\pi v_{\perp} dv_{\perp}$, $J_n = J_n(\mu_s)$ is the Bessel function of the first kind of order n (for $n = 0, \pm 1, \pm 2, \dots$), and $J'_n = dJ_n(\mu_s)/d\mu_s$ denotes its derivative. The argument μ_s is given by $\mu_s = k_{\perp} v_{\perp} / \omega_{cs}$, with the gyrofrequency $\omega_{cs} = q_s B_0 / m_s$, and plasma frequency $\omega_{ps} = \sqrt{n_{0s} q_s^2 / (\epsilon_0 m_s)}$. Here, q_s , m_s and n_{0s} are particle

charge, mass and number density, respectively. We define the A_s and B_s by

$$A_s \equiv \left[\left(1 - \frac{k_{\parallel} v_{\parallel}}{\omega} \right) \frac{\partial}{\partial v_{\perp}} + \frac{k_{\parallel} v_{\perp}}{\omega} \frac{\partial}{\partial v_{\parallel}} \right] f_{s0}, \quad (8a)$$

$$B_s \equiv \left[\frac{n\omega_{cs}}{\omega} \left(\frac{v_{\parallel}}{v_{\perp}} \right) \frac{\partial}{\partial v_{\perp}} + \left(1 - \frac{n\omega_{cs}}{\omega} \right) \frac{\partial}{\partial v_{\parallel}} \right] f_{s0}. \quad (8b)$$

To further derive the expression for the susceptibility χ , we use the modified plasma dispersion function introduced by Summers and Thorne [6], defined as

$$Z_{\kappa_{\parallel s}}(\xi_n) = \frac{\Gamma(\kappa_{\parallel s} + 1)}{\sqrt{\pi} \kappa_{\parallel s}^3 \Gamma(\kappa_{\parallel s} - 1/2)} \int_{-\infty}^{\infty} \frac{dx}{(x - \xi_n) \left(1 + x^2/\kappa_{\parallel s} \right)^{\kappa_{\parallel s} + 1}}, \quad \Im(\xi) > 0, \quad (9)$$

with $x = (v_{\parallel} - u_{s0})/\theta_{\parallel s}$ and $\xi_n = (\omega - n\omega_{cs} - k_{\parallel} u_{s0})/k_{\parallel} \theta_{\parallel s}$. For any positive integer $\kappa_{\parallel s}$, and all $\xi_n \neq \pm i\sqrt{\kappa_{\parallel s}}$, the expressions for these dispersion functions can be given using closed-form expansions [24, 7],

$$Z_{\kappa_{\parallel s}}(\xi_n) = \frac{i(\kappa_{\parallel s} - 1/2)}{2\kappa_{\parallel s}^{3/2}} \frac{\kappa_{\parallel s}!}{(2\kappa_{\parallel s})!} \sum_{l=1}^{\kappa_{\parallel s}+1} \frac{(\kappa_{\parallel s} + l - 1)!}{(l - 1)!} \left(\frac{2i}{(\xi_n/\sqrt{\kappa_{\parallel s}}) + i} \right)^{\kappa_{\parallel s} - l + 2}. \quad (10)$$

We define $\mathcal{Z}_{\kappa_{\parallel s}} \equiv Z_{\kappa_{\parallel s}} / [1 - 1/(2\kappa_{\parallel s})]$ and $\mathcal{Z}'_{\kappa_{\parallel s}} \equiv \partial \mathcal{Z}_{\kappa_{\parallel s}} / \partial \xi_n$. The closed-form expressions are given by

$$\mathcal{Z}_{\kappa_{\parallel s}} = \frac{i}{2\sqrt{\kappa_{\parallel s}}} \frac{\kappa_{\parallel s}!}{(2\kappa_{\parallel s})!} \sum_{l=1}^{\kappa_{\parallel s}+1} \frac{(\kappa_{\parallel s} + l - 1)!}{(l - 1)!} \left(\frac{2i}{(\xi_n/\sqrt{\kappa_{\parallel s}}) + i} \right)^{\kappa_{\parallel s} - l + 2}, \quad (11a)$$

$$\mathcal{Z}'_{\kappa_{\parallel s}} = -\frac{(\kappa_{\parallel s} + 1/2)}{\kappa_{\parallel s}} \frac{(\kappa_{\parallel s} + 1)!}{(2\kappa_{\parallel s} + 2)!} \sum_{l=1}^{\kappa_{\parallel s}+1} (\kappa_{\parallel s} - l + 2) \frac{(\kappa_{\parallel s} + l - 1)!}{(l - 1)!} \left(\frac{2i}{(\xi_n/\sqrt{\kappa_{\parallel s}}) + i} \right)^{\kappa_{\parallel s} - l + 3}. \quad (11b)$$

Following the derivation, the susceptibility components χ_{ij} for a PBK plasma are

$$\chi_{11}^{\text{PBK}} = - \sum_s \frac{\omega_{ps}^2}{\omega^2} + \sum_{sn} \frac{\omega_{ps}^2}{\omega^2} n^2 C_{12sn}^{\text{PBK}}, \quad (12a)$$

$$\chi_{12}^{\text{PBK}} = i \sum_{sn} \frac{\omega_{ps}^2}{\omega^2} n C_{34sn}^{\text{PBK}}, \quad (12b)$$

$$\chi_{13}^{\text{PBK}} = \tan \theta \left[\sum_s \frac{\omega_{ps}^2}{\omega^2} + \sum_{sn} \frac{\omega_{ps}^2}{\omega^2} n \left(\frac{\omega - n\omega_{cs}}{\omega_{cs}} \right) C_{12sn}^{\text{PBK}} \right], \quad (12c)$$

$$\chi_{22}^{\text{PBK}} = - \sum_s \frac{\omega_{ps}^2}{\omega^2} + \sum_{sn} \frac{\omega_{ps}^2}{\omega^2} C_{56sn}^{\text{PBK}}, \quad (12d)$$

$$\chi_{23}^{\text{PBK}} = -i \tan \theta \sum_{sn} \frac{\omega_{ps}^2}{\omega^2} \left(\frac{\omega - n\omega_{cs}}{\omega_{cs}} \right) C_{34sn}^{\text{PBK}}, \quad (12e)$$

$$\chi_{33}^{\text{PBK}} = \tan^2 \theta \left[- \sum_s \frac{\omega_{ps}^2}{\omega^2} + \sum_{sn} \frac{\omega_{ps}^2}{\omega^2} \left(\frac{\omega - n\omega_{cs}}{\omega_{cs}} \right)^2 C_{12sn}^{\text{PBK}} \right], \quad (12f)$$

where $\chi_{12}^{\text{PBK}} = -\chi_{21}^{\text{PBK}}$, $\chi_{13}^{\text{PBK}} = \chi_{31}^{\text{PBK}}$, and $\chi_{23}^{\text{PBK}} = -\chi_{32}^{\text{PBK}}$. Using the closed forms in Eqs. (11a) and (11b), the coefficients C_{12sn}^{PBK} , C_{34sn}^{PBK} , and C_{56sn}^{PBK} take the simplified rational form

$$C_{12sn}^{\text{PBK}} = \left(\frac{n\omega_{cs}}{k_{\parallel} \theta_{\parallel s}} \right) S_{17} \mathcal{Z}_{\kappa_{\parallel s}} - \left(\frac{\theta_{\perp s}^2}{2\theta_{\parallel s}^2} \right) S_2 \mathcal{Z}'_{\kappa_{\parallel s}} = \sum_{l=1}^{\kappa_{\parallel s}} \left[\frac{b_{1snl}}{(\omega - c_{sn})^l} + \frac{b_{2snl}}{(\omega - c_{sn})^{l+1}} \right], \quad (13a)$$

$$C_{34sn}^{\text{PBK}} = \left(\frac{n\omega_{cs}}{k_{\parallel} \theta_{\parallel s}} \right) S_{38} \mathcal{Z}_{\kappa_{\parallel s}} - \left(\frac{\theta_{\perp s}^2}{2\theta_{\parallel s}^2} \right) S_4 \mathcal{Z}'_{\kappa_{\parallel s}} = \sum_{l=1}^{\kappa_{\parallel s}} \left[\frac{b_{3snl}}{(\omega - c_{sn})^l} + \frac{b_{4snl}}{(\omega - c_{sn})^{l+1}} \right], \quad (13b)$$

$$C_{56sn}^{\text{PBK}} = \left(\frac{n\omega_{cs}}{k_{\parallel} \theta_{\parallel s}} \right) S_{59} \mathcal{Z}_{\kappa_{\parallel s}} - \left(\frac{\theta_{\perp s}^2}{2\theta_{\parallel s}^2} \right) S_6 \mathcal{Z}'_{\kappa_{\parallel s}} = \sum_{l=1}^{\kappa_{\parallel s}} \left[\frac{b_{5snl}}{(\omega - c_{sn})^l} + \frac{b_{6snl}}{(\omega - c_{sn})^{l+1}} \right]. \quad (13c)$$

where,

$$\left\{ \begin{array}{l} b_{1snl} = S_{17}b_{snl}, \quad b_{3snl} = S_{38}b_{snl}, \quad b_{5snl} = S_{59}b_{snl}, \\ b_{2snl} = S_2b_{sl}, \quad b_{4snl} = S_4b_{sl}, \quad b_{6snl} = S_6b_{sl}, \\ S_{17} = \left(\frac{\kappa_{\perp s} + \sigma_s + 1}{\kappa_{\perp s}} \right) S_1 - 2\sigma_s \lambda_s S_7, \\ S_{38} = \left(\frac{\kappa_{\perp s} + \sigma_s + 1}{\kappa_{\perp s}} \right) S_3 - 2\sigma_s \lambda_s S_8, \\ S_{59} = \left(\frac{\kappa_{\perp s} + \sigma_s + 1}{\kappa_{\perp s}} \right) S_5 - 2\sigma_s \lambda_s S_9, \\ b_{sl} = -\frac{l}{2} k_{\parallel}^2 \theta_{\perp s}^2 c_{sl}, \quad b_{snl} = -n\omega_{cs} c_{sl}, \\ c_{sn} = n\omega_{cs} + k_{\parallel} u_{s0} - i\sqrt{\kappa_{\parallel s}} k_{\parallel} \theta_{\parallel s}, \\ c_{sl} = \frac{\Gamma(\kappa_{\parallel s} + 1)\Gamma(2\kappa_{\parallel s} - l + 2)}{\Gamma(2\kappa_{\parallel s} + 1)\Gamma(\kappa_{\parallel s} - l + 2)} (2i\sqrt{\kappa_{\parallel s}} k_{\parallel} \theta_{\parallel s})^{l-1}, \end{array} \right. \quad (14)$$

and $(c_{sl})_{l=1} = 1$. The unified integral expression is given by

$$S_{\kappa_{\perp s}}(p_1, p_2, p_3, p_4) = S_0 \int_0^\infty \frac{J_n^{p_1}(\mu_s) J_n'^{p_2}(\mu_s) \mu_s^{2\sigma_s + p_3}}{\left(1 + \frac{\mu_s^2}{2\lambda_s \kappa_{\perp s}}\right)^{\kappa_{\perp s} + \sigma_s + p_4}} d\mu_s, \quad (15a)$$

$$S_0 = \frac{4\Gamma(\kappa_{\perp s} + \sigma_s + 1)}{(2\lambda_s)^{\sigma_s + 2} (\kappa_{\perp s})^{\sigma_s + 1} \Gamma(\kappa_{\perp s}) \Gamma(\sigma_s + 1)}, \quad (15b)$$

where $\lambda_s = \frac{k_{\perp}^2 \theta_{\perp s}^2}{2\omega_{cs}^2}$, $J_n^{p_1}(\mu_s) = [J_n(\mu_s)]^{p_1}$, and $J_n'^{p_2}(\mu_s) = \left[\frac{dJ_n(\mu_s)}{d\mu_s} \right]^{p_2}$. In terms of this expression, the nine integrals in equation set (13) can be compactly written as

$$\left\{ \begin{array}{l} S_1 = S_{\kappa_{\perp s}}(2, 0, 1, 2), \quad S_2 = S_{\kappa_{\perp s}}(2, 0, 1, 1), \quad S_3 = S_{\kappa_{\perp s}}(1, 1, 2, 2), \\ S_4 = S_{\kappa_{\perp s}}(1, 1, 2, 1), \quad S_5 = S_{\kappa_{\perp s}}(0, 2, 3, 2), \quad S_6 = S_{\kappa_{\perp s}}(0, 2, 3, 1), \\ S_7 = S_{\kappa_{\perp s}}(2, 0, -1, 1), \quad S_8 = S_{\kappa_{\perp s}}(1, 1, 0, 1), \quad S_9 = S_{\kappa_{\perp s}}(0, 2, 1, 1). \end{array} \right. \quad (16)$$

When computing the integrals in Eq. (15a) numerically, care must be taken to prevent numerical overflow due to large value of $\kappa_{\perp s}$, for enhanced stability, the coefficient S_0 should be evaluated in its logarithmic form $S_0 = \frac{4 \exp[\ln \Gamma(\kappa_{\perp s} + \sigma_s + 1) - \ln \Gamma(\kappa_{\perp s})]}{(2\lambda_s)^{\sigma_s + 2} (\kappa_{\perp s})^{\sigma_s + 1} \Gamma(\sigma_s + 1)}$. Handing the $\lambda_s \rightarrow 0$ limit requires a change of the integration variable $\hat{\mu} = \mu/\sqrt{2\lambda_s}$ [7] for numerical stability, as the integral

(15a) becomes critical when $k_{\perp} \rightarrow 0$ or $\theta_{\perp s} \rightarrow 0$. This yields the transformed integral

$$S_{\kappa_{\perp s}}(p_1, p_2, p_3, p_4) = \hat{S}_0 \int_0^\infty \frac{J_n^{p_1}(\sqrt{2\lambda_s}\hat{\mu}) J_n^{p_2}(\sqrt{2\lambda_s}\hat{\mu}) \hat{\mu}^{2\sigma_s+p_3}}{\left(1 + \frac{\hat{\mu}^2}{\kappa_{\perp s}}\right)^{\kappa_{\perp s}+\sigma_s+p_4}} d\hat{\mu}, \quad (17)$$

where $\hat{S}_0 = \frac{4 \exp[\ln \Gamma(\kappa_{\perp s}+\sigma_s+1) - \ln \Gamma(\kappa_{\perp s})]}{(2\lambda_s)^{(3-p_3)/2} (\kappa_{\perp s})^{\sigma_s+1} \Gamma(\sigma_s+1)}$.

2.3. Susceptibility tensors in the Maxwellian limit

In the Maxwellian limit ($\kappa_{\perp s} \rightarrow \infty$), the coefficients given by equation set (13) become

$$\left\{ \begin{array}{l} \lim_{\kappa_{\perp s} \rightarrow \infty} C_{12sn}^{\text{PBK}} = \left(\frac{n\omega_{cs}}{k_{\parallel} \theta_{\parallel s}} \right) \tilde{S}_{17} \mathcal{Z}_{\kappa_{\parallel s}} - \left(\frac{\theta_{\perp s}^2}{2\theta_{\parallel s}^2} \right) \tilde{S}_2 \mathcal{Z}'_{\kappa_{\parallel s}} = \sum_{l=1}^{\kappa_{\parallel s}} \left[\frac{\tilde{b}_{1snl}}{(\omega - c_{sn})^l} + \frac{\tilde{b}_{2snl}}{(\omega - c_{sn})^{l+1}} \right], \\ \lim_{\kappa_{\perp s} \rightarrow \infty} C_{34sn}^{\text{PBK}} = \left(\frac{n\omega_{cs}}{k_{\parallel} \theta_{\parallel s}} \right) \tilde{S}_{38} \mathcal{Z}_{\kappa_{\parallel s}} - \left(\frac{\theta_{\perp s}^2}{2\theta_{\parallel s}^2} \right) \tilde{S}_4 \mathcal{Z}'_{\kappa_{\parallel s}} = \sum_{l=1}^{\kappa_{\parallel s}} \left[\frac{\tilde{b}_{3snl}}{(\omega - c_{sn})^l} + \frac{\tilde{b}_{4snl}}{(\omega - c_{sn})^{l+1}} \right], \\ \lim_{\kappa_{\perp s} \rightarrow \infty} C_{56sn}^{\text{PBK}} = \left(\frac{n\omega_{cs}}{k_{\parallel} \theta_{\parallel s}} \right) \tilde{S}_{59} \mathcal{Z}_{\kappa_{\parallel s}} - \left(\frac{\theta_{\perp s}^2}{2\theta_{\parallel s}^2} \right) \tilde{S}_6 \mathcal{Z}'_{\kappa_{\parallel s}} = \sum_{l=1}^{\kappa_{\parallel s}} \left[\frac{\tilde{b}_{5snl}}{(\omega - c_{sn})^l} + \frac{\tilde{b}_{6snl}}{(\omega - c_{sn})^{l+1}} \right], \end{array} \right. \quad (18)$$

where

$$\left\{ \begin{array}{l} \tilde{b}_{1snl} = \tilde{S}_{17} b_{snl}, \quad \tilde{b}_{3snl} = \tilde{S}_{38} b_{snl}, \quad \tilde{b}_{5snl} = \tilde{S}_{59} b_{snl}, \\ \tilde{b}_{2snl} = \tilde{S}_2 b_{sl}, \quad \tilde{b}_{4snl} = \tilde{S}_4 b_{sl}, \quad \tilde{b}_{6snl} = \tilde{S}_6 b_{sl}, \quad \tilde{S}_0 = \frac{4}{(2\lambda_s)^{\sigma_s+2} \Gamma(\sigma_s+1)}, \\ \tilde{S}_1 = \tilde{S}_2 = \tilde{S}_0 \int_0^\infty J_n^2 \mu_s^{2\sigma_s+1} \exp\left(-\frac{\mu_s^2}{2\lambda_s}\right) d\mu_s, \quad \tilde{S}_1 \Big|_{\sigma_s=0} = \tilde{S}_2 \Big|_{\sigma_s=0} = \Lambda_n / \lambda_s, \\ \tilde{S}_3 = \tilde{S}_4 = \tilde{S}_0 \int_0^\infty J_n J'_n \mu_s^{2\sigma_s+2} \exp\left(-\frac{\mu_s^2}{2\lambda_s}\right) d\mu_s, \quad \tilde{S}_3 \Big|_{\sigma_s=0} = \tilde{S}_4 \Big|_{\sigma_s=0} = \Lambda'_n, \\ \tilde{S}_5 = \tilde{S}_6 = \tilde{S}_0 \int_0^\infty J'_n^2 \mu_s^{2\sigma_s+3} \exp\left(-\frac{\mu_s^2}{2\lambda_s}\right) d\mu_s, \quad \tilde{S}_5 \Big|_{\sigma_s=0} = \tilde{S}_6 \Big|_{\sigma_s=0} = n^2 \Lambda_n / \lambda_s - 2\lambda_s \Lambda'_n, \\ \tilde{S}_7 = \tilde{S}_0 \int_0^\infty J_n^2 \mu_s^{2\sigma_s-1} \exp\left(-\frac{\mu_s^2}{2\lambda_s}\right) d\mu_s, \quad \tilde{S}_8 = \tilde{S}_0 \int_0^\infty J_n J'_n \mu_s^{2\sigma_s} \exp\left(-\frac{\mu_s^2}{2\lambda_s}\right) d\mu_s, \\ \tilde{S}_9 = \tilde{S}_0 \int_0^\infty J'_n^2 \mu_s^{2\sigma_s+1} \exp\left(-\frac{\mu_s^2}{2\lambda_s}\right) d\mu_s, \quad \tilde{S}_{17} = (\tilde{S}_1 - 2\sigma_s \lambda_s \tilde{S}_7), \\ \tilde{S}_{38} = (\tilde{S}_3 - 2\sigma_s \lambda_s \tilde{S}_8), \quad \tilde{S}_{59} = (\tilde{S}_5 - 2\sigma_s \lambda_s \tilde{S}_9), \end{array} \right. \quad (19)$$

with $\Lambda_n = I_n(\lambda_s) \exp(-\lambda_s)$ and $\Lambda'_s = d\Lambda/d\lambda_s$, where I_n is the modified Bessel function of the first of order n . Substituting the coefficients from equation set (18) into the PBK susceptibility χ_{ij}^{PBK} in equation set (12) yields the susceptibility components for the loss-cone drift KM plasma. In particular, for $\sigma_s = 0$, the relations for $\tilde{S}_1|_{\sigma_s=0}$ to $\tilde{S}_6|_{\sigma_s=0}$ from Eqs. (19) simplify the result to

$$\begin{cases} \lim_{\kappa_{\perp s} \rightarrow \infty} C_{12sn}^{\text{PBK}}|_{\sigma_s=0} = \frac{I_n e^{-\lambda_s}}{\lambda_s} C_n, \\ \lim_{\kappa_{\perp s} \rightarrow \infty} C_{34sn}^{\text{PBK}}|_{\sigma_s=0} = -(I_n - I'_n) e^{-\lambda_s} C_n, \\ \lim_{\kappa_{\perp s} \rightarrow \infty} C_{56sn}^{\text{PBK}}|_{\sigma_s=0} = \frac{[n^2 I_n + 2\lambda_s^2 (I_n - I'_n)] e^{-\lambda_s}}{\lambda_s} C_n, \end{cases} \quad (20)$$

where $C_n = \left(\frac{n\omega_{cs}}{k_{\parallel} \theta_{\parallel s}} \right) \mathcal{Z}_{\kappa_{\parallel s}} - \left(\frac{\theta_{\perp s}^2}{2\theta_{\parallel s}^2} \right) \mathcal{Z}'_{\kappa_{\parallel s}}$. Substituting equation set (20) into the general susceptibility χ_{ij}^{PBK} in Eq. (12), yields a KM susceptibility tensor that reproduces the result in Refs. [13, 25]:

$$\begin{cases} \chi_{11}^{\text{KM}}|_{\sigma_s=0} = - \sum_s \frac{\omega_{ps}^2}{\omega^2} + \sum_{sn} \frac{\omega_{ps}^2}{\omega^2} n^2 \frac{I_n e^{-\lambda_s}}{\lambda_s} C_n, \\ \chi_{12}^{\text{KM}}|_{\sigma_s=0} = -i \sum_{sn} \frac{\omega_{ps}^2}{\omega^2} n (I_n - I'_n) e^{-\lambda_s} C_n, \\ \chi_{13}^{\text{KM}}|_{\sigma_s=0} = \tan \theta \left[\sum_s \frac{\omega_{ps}^2}{\omega^2} + \sum_{sn} \frac{\omega_{ps}^2}{\omega^2} \left(\frac{\omega - n\omega_{cs}}{\omega_{cs}} \right) n \frac{I_n e^{-\lambda_s}}{\lambda_s} C_n \right], \\ \chi_{22}^{\text{KM}}|_{\sigma_s=0} = - \sum_s \frac{\omega_{ps}^2}{\omega^2} + \sum_{sn} \frac{\omega_{ps}^2}{\omega^2} \frac{[n^2 I_n + 2\lambda_s^2 (I_n - I'_n)] e^{-\lambda_s}}{\lambda_s} C_n, \\ \chi_{23}^{\text{KM}}|_{\sigma_s=0} = i \tan \theta \sum_{sn} \frac{\omega_{ps}^2}{\omega^2} \left(\frac{\omega - n\omega_{cs}}{\omega_{cs}} \right) (I_n - I'_n) e^{-\lambda_s} C_n, \\ \chi_{33}^{\text{KM}}|_{\sigma_s=0} = \tan^2 \theta \left[- \sum_s \frac{\omega_{ps}^2}{\omega^2} + \sum_{sn} \frac{\omega_{ps}^2}{\omega^2} \left(\frac{\omega - n\omega_{cs}}{\omega_{cs}} \right)^2 \frac{I_n e^{-\lambda_s}}{\lambda_s} C_n \right]. \end{cases} \quad (21)$$

In Maxwellian limit ($\kappa_{\parallel s} \rightarrow \infty$), the modified plasma dispersion function converges to its standard form, $\lim_{\kappa_{\parallel s} \rightarrow \infty} \mathcal{Z}_{\kappa_{\parallel s}}(\xi) = Z(\xi)$, $\lim_{\kappa_{\parallel s} \rightarrow \infty} \mathcal{Z}'_{\kappa_{\parallel s}}(\xi) = Z'(\xi) = -2[1 + \xi Z(\xi)]$. The Maxwellian plasma dispersion, $Z(\xi) = \frac{1}{\sqrt{\pi}} \int_{-\infty}^{\infty} \frac{e^{-z^2}}{z - \xi} dz$ is efficiently computed via the Padé approximation method with the J -pole expansion [32], $Z(\xi) \approx Z_J(\xi) = \sum_{j=1}^J \frac{b_j}{\xi - c_j}$, where the coefficients b_j and c_j are

tabulated by Xie et al. [20]. For subsequent derivations, we further employ the relations from [21] $\sum_j b_j = -1$, $\sum_j b_j c_j = 0$, and $\sum_j b_j c_j^2 = -1/2$. When both $\kappa_{\parallel s} \rightarrow \infty$ and $\kappa_{\perp s} \rightarrow \infty$, the coefficients in equation set (13) reduce to

$$\begin{cases} \lim_{\kappa_{\parallel s}, \kappa_{\perp s} \rightarrow \infty} C_{12sn}^{\text{PBK}} = \left(\frac{n\omega_{cs}}{k_{\parallel} \theta_{\parallel s}} \right) \tilde{S}_{17} Z(\xi_n) - \left(\frac{\theta_{\perp s}^2}{2\theta_{\parallel s}^2} \right) \tilde{S}_2 Z'(\xi_n) = \sum_{j=1}^J \frac{\tilde{b}_{12snj}}{\omega - \tilde{c}_{snj}}, \\ \lim_{\kappa_{\parallel s}, \kappa_{\perp s} \rightarrow \infty} C_{34sn}^{\text{PBK}} = \left(\frac{n\omega_{cs}}{k_{\parallel} \theta_{\parallel s}} \right) \tilde{S}_{38} Z(\xi_n) - \left(\frac{\theta_{\perp s}^2}{2\theta_{\parallel s}^2} \right) \tilde{S}_4 Z'(\xi_n) = \sum_{j=1}^J \frac{\tilde{b}_{34snj}}{\omega - \tilde{c}_{snj}}, \\ \lim_{\kappa_{\parallel s}, \kappa_{\perp s} \rightarrow \infty} C_{56sn}^{\text{PBK}} = \left(\frac{n\omega_{cs}}{k_{\parallel} \theta_{\parallel s}} \right) \tilde{S}_{59} Z(\xi_n) - \left(\frac{\theta_{\perp s}^2}{2\theta_{\parallel s}^2} \right) \tilde{S}_6 Z'(\xi_n) = \sum_{j=1}^J \frac{\tilde{b}_{56snj}}{\omega - \tilde{c}_{snj}}, \end{cases} \quad (22)$$

where

$$\begin{cases} \tilde{c}_{snj} = n\omega_{cs} + k_{\parallel} u_{s0} + c_j k_{\parallel} \theta_{\parallel s}, \\ \tilde{b}_{12snj} = n\omega_{cs} b_j \tilde{S}_{17} + b_j c_j k_{\parallel} \theta_{\parallel s} \frac{T_{\perp s} \tilde{S}_2}{T_{\parallel s}(\sigma_s + 1)}, \\ \tilde{b}_{34snj} = n\omega_{cs} b_j \tilde{S}_{38} + b_j c_j k_{\parallel} \theta_{\parallel s} \frac{T_{\perp s} \tilde{S}_4}{T_{\parallel s}(\sigma_s + 1)}, \\ \tilde{b}_{56snj} = n\omega_{cs} b_j \tilde{S}_{59} + b_j c_j k_{\parallel} \theta_{\parallel s} \frac{T_{\perp s} \tilde{S}_6}{T_{\parallel s}(\sigma_s + 1)}. \end{cases} \quad (23)$$

Substituting the coefficients from equation set (22) into the PBK susceptibility χ_{ij}^{PBK} in equation set (12), yields all susceptibility components for the loss-cone drift BM plasma.

3. Equivalent linear system for the BO-PBK solver

The Vlasov-Maxwell system provides a complete kinetic description of particle-electromagnetic field interactions in plasmas. From its linearized equations, one derives a general dispersion relation for linear wave modes. Within this self-consistent theoretical framework, we have developed a novel numerical solver for kinetic waves in a uniformly magnetized plasma under the small-amplitude perturbations. The solver models the plasma as a responsive medium characterized by a conductivity tensor derived from the linearized Vlasov-Maxwell equations. Integrating the tensor into Maxwell's equations via the Ohm's law yields a closed linear system for solving the

plasma wave and instability modes. The perturbation Maxwell's equations are

$$\nabla \times \delta \mathbf{E} = -\frac{\partial \delta \mathbf{B}}{\partial t}, \quad (24a)$$

$$\nabla \times \delta \mathbf{B} = \mu_0 \delta \mathbf{J} + \mu_0 \epsilon_0 \frac{\partial \delta \mathbf{E}}{\partial t} = \mu_0 \epsilon_0 \boldsymbol{\epsilon} \cdot \frac{\partial \delta \mathbf{E}}{\partial t}. \quad (24b)$$

The conductivity tensor $\boldsymbol{\sigma} = -i\epsilon_0\omega\boldsymbol{\chi}$ defines the dielectric tensor $\boldsymbol{\epsilon} = \boldsymbol{\mathcal{I}} + \frac{i}{\epsilon_0\omega}\boldsymbol{\sigma}$. The current density response in the frequency domain is then

$$\begin{pmatrix} \delta J_x \\ \delta J_y \\ \delta J_z \end{pmatrix} = -i\epsilon_0\omega \begin{pmatrix} \chi_{11} & \chi_{12} & \chi_{13} \\ \chi_{21} & \chi_{22} & \chi_{23} \\ \chi_{31} & \chi_{32} & \chi_{33} \end{pmatrix} \begin{pmatrix} \delta E_x \\ \delta E_y \\ \delta E_z \end{pmatrix}, \quad (25)$$

where $\chi_{ij} = \sum_{s=1}^{S_{\text{PBK}}} \chi_{s,ij}^{\text{PBK}} + \sum_{s=1}^{S_{\text{KM}}} \chi_{s,ij}^{\text{KM}}$. Here, S_{PBK} and S_{KM} denote the number of PBK and KM particle species, respectively, and $S = S_{\text{PBK}} + S_{\text{KM}}$ represents the total number of species. The PBK model generalizes the BM model, which is recovered as $\kappa \rightarrow \infty$ [24, 33]. To analyze electromagnetic waves propagation, we apply the Fourier ansatz $\partial/\partial t = -i\omega$ to Maxwell's equations (24a), (24b), yielding the dispersion relation $\det(\mathbf{kk} - k^2\boldsymbol{\mathcal{I}} + \frac{\omega^2}{c^2}\boldsymbol{\epsilon}) = 0$. Instead of employing iterative root-finding algorithms (such as the shooting or Müller method) with initial guesses for ω , we reformulate the system of equations (24a), (24b), (25) as a linear eigenvalue problem. This approach constructs a unified linear system, detailed in the following section.

3.1. Equivalent linear system for PBK and KM plasmas

The perturbed current in the x -direction, derived from Eqs. (13a), (13b), (12a), (12b), (12c) and Ohm's law (25), is

$$\begin{aligned} \delta J_x^{\text{PBK}} = & \frac{b_{x10}}{\omega} \delta E_x + \sum_{sn} \sum_{l=1}^{\kappa_{\parallel s}} \frac{b_{x33sn,l+1}}{\omega(\omega - c_{sn})^l} \delta E_z \\ & + \sum_{sn} \sum_{l=1}^{\kappa_{\parallel s}+1} \left[\frac{b_{x11snl}}{\omega(\omega - c_{sn})^l} \delta E_x + \frac{b_{x21snl}}{\omega(\omega - c_{sn})^l} \delta E_y + \frac{b_{x31snl}}{\omega(\omega - c_{sn})^l} \delta E_z \right] \\ & + \sum_{sn} \sum_{l=1}^{\kappa_{\parallel s}+1} \left[\frac{b_{x12snl}}{\omega(\omega - c_{sn})^{l+1}} \delta E_x + \frac{b_{x22snl}}{\omega(\omega - c_{sn})^{l+1}} \delta E_y + \frac{b_{x32snl}}{\omega(\omega - c_{sn})^{l+1}} \delta E_z \right], \end{aligned} \quad (26)$$

where

$$\left\{ \begin{array}{l} b_{x10} = i\epsilon_0 \sum_s \omega_{ps}^2, \quad b_{x30} = -i\epsilon_0 \tan \theta \sum_s \omega_{ps}^2, \quad b_{x11snl} = -i\epsilon_0 \omega_{ps}^2 n^2 b_{1snl}, \\ b_{x12snl} = -i\epsilon_0 \omega_{ps}^2 n^2 b_{2snl}, \quad b_{x21snl} = \epsilon_0 \omega_{ps}^2 n b_{3snl}, \quad b_{x22snl} = \epsilon_0 \omega_{ps}^2 n b_{4snl}, \\ b_{x31snl} = -i\epsilon_0 \tan \theta \omega_{ps}^2 n \left[\frac{(c_{sn} - n\omega_{cs}) b_{1snl} + b_{2snl}}{\omega_{cs}} \right], \\ b_{x32snl} = -i\epsilon_0 \tan \theta \omega_{ps}^2 n \left[\frac{(c_{sn} - n\omega_{cs}) b_{2snl}}{\omega_{cs}} \right], \\ b_{x33snl} = -i\epsilon_0 \tan \theta \omega_{ps}^2 n \frac{b_{1snl}}{\omega_{cs}}, \quad \sum_{sn} b_{x33snl} = -b_{x30}. \end{array} \right. \quad (27)$$

Furthermore, Eq. (26) leads to the linear eigenvalue problem $\omega \mathbf{x} = \mathbf{M}_x \mathbf{x}$. Expanding this system yields,

$$\left\{ \begin{array}{l} \omega \delta J_x^{\text{PBK}} = b_{x10} \delta E_x + \sum_{sn} \sum_{l=1}^{\kappa_{\parallel s} + 1} x_{snl1}, \\ \omega x_{snl1} = c_{sn} x_{snl1} + x_{snl2}, \\ \vdots \\ \omega x_{snl,l-1} = c_{sn} x_{snl,l-1} + x_{snll}, \\ \omega x_{snll} = \left\{ \begin{array}{l} b_{x33sn,l+1} \delta E_z + b_{x11snl} \delta E_x + b_{x21snl} \delta E_y + b_{x31snl} \delta E_z \\ + c_{sn} x_{snll} + x_{snl,l+1}, \text{ (if } l \leq \kappa_{\parallel s}), \\ b_{x11snl} \delta E_x + b_{x21snl} \delta E_y + b_{x31snl} \delta E_z + c_{sn} x_{snll} + x_{snl,l+1}, \text{ (if } l = \kappa_{\parallel s} + 1), \end{array} \right. \\ \omega x_{snl,l+1} = b_{x12snl} \delta E_x + b_{x22snl} \delta E_y + b_{x32snl} \delta E_z + c_{sn} x_{snl,l+1}, \end{array} \right. \quad (28)$$

The vector is defined as $\mathbf{x} = [x_{snl1}, x_{snl2}, \dots, x_{snl,l+1}, \delta J_x^{\text{PBK}}]^T$, and therefore the total number of equations in linear system (28) is $N_x^{\text{PBK}} = 1 + \sum_{s=1}^{S_{\text{PBK}}} \sum_{n=-N_s}^{N_s} \sum_{l=1}^{\kappa_{\parallel s} + 1} (l + 1)$.

Similarly, the perturbed current in the y -direction is given by

$$\begin{aligned} \delta J_y^{\text{PBK}} = & \frac{b_{y20}}{\omega} \delta E_y + \sum_{sn} \sum_{l=1}^{\kappa_{\parallel s}} \frac{b_{y33sn,l+1}}{\omega (\omega - c_{sn})^l} \delta E_z, \\ & + \sum_{sn} \sum_{l=1}^{\kappa_{\parallel s} + 1} \left[\frac{b_{y11snl}}{\omega (\omega - c_{sn})^l} \delta E_x + \frac{b_{y21snl}}{\omega (\omega - c_{sn})^l} \delta E_y + \frac{b_{y31snl}}{\omega (\omega - c_{sn})^l} \delta E_z \right] \\ & + \sum_{sn} \sum_{l=1}^{\kappa_{\parallel s} + 1} \left[\frac{b_{y12snl}}{\omega (\omega - c_{sn})^{l+1}} \delta E_x + \frac{b_{y22snl}}{\omega (\omega - c_{sn})^{l+1}} \delta E_y + \frac{b_{y32snl}}{\omega (\omega - c_{sn})^{l+1}} \delta E_z \right], \end{aligned} \quad (29)$$

as derived from Eqs. (13a), (13b), (13c), (12b), (12d), (12e), and (25). The coefficients are

$$\left\{ \begin{array}{l} b_{y20} = i\epsilon_0 \sum_s \omega_{ps}^2, \quad b_{y11snl} = -\epsilon_0 \omega_{ps}^2 n b_{3snl}, \quad b_{y12snl} = -\epsilon_0 \omega_{ps}^2 n b_{4snl}, \\ b_{y21snl} = -i\epsilon_0 \omega_{ps}^2 b_{5snl}, \quad b_{y22snl} = -i\epsilon_0 \omega_{ps}^2 b_{6snl}, \\ b_{y31snl} = -\epsilon_0 \tan \theta \omega_{ps}^2 \left[\frac{(c_{sn} - n\omega_{cs}) b_{3snl} + b_{4snl}}{\omega_{cs}} \right], \\ b_{y32snl} = -\epsilon_0 \tan \theta \omega_{ps}^2 \left[\frac{(c_{sn} - n\omega_{cs}) b_{4snl}}{\omega_{cs}} \right], \\ b_{y33snl} = -\epsilon_0 \tan \theta \omega_{ps}^2 \left(\frac{b_{3snl}}{\omega_{cs}} \right), \quad \sum_{sn} b_{y33snl} = 0. \end{array} \right. \quad (30)$$

Applying the same method to Eq. (29) yields the linear system for the y -direction $\omega \mathbf{y} = \mathbf{M}_y \mathbf{y}$, its explicit form is provided below

$$\left\{ \begin{array}{l} \omega \delta J_y^{\text{PBK}} = b_{y20} \delta E_y + \sum_{sn} \sum_{l=1}^{\kappa_{\parallel s} + 1} y_{snl1}, \\ \omega y_{snl1} = c_{sn} y_{snl1} + y_{snl2}, \\ \vdots \\ \omega y_{snl,l-1} = c_{sn} y_{snl,l-1} + y_{snll}, \\ \omega y_{snll} = \left\{ \begin{array}{l} b_{y33sn,l+1} \delta E_z + b_{y11snl} \delta E_x + b_{y21snl} \delta E_y + b_{y31snl} \delta E_z \\ + c_{sn} y_{snll} + y_{snl,l+1}, \text{ (if } l \leq \kappa_{\parallel s}), \\ b_{y11snl} \delta E_x + b_{y21snl} \delta E_y + b_{y31snl} \delta E_z + c_{sn} y_{snll} + y_{snl,l+1}, \text{ (if } l = \kappa_{\parallel s} + 1), \end{array} \right. \\ \omega y_{snl,l+1} = b_{y12snl} \delta E_x + b_{y22snl} \delta E_y + b_{y32snl} \delta E_z + c_{sn} y_{snl,l+1}, \end{array} \right. \quad (31)$$

where $\mathbf{y} = [y_{snl1}, y_{snl2}, \dots, y_{snl,l+1}, \delta J_y^{\text{PBK}}]^T$, the total number of equations in linear system (31) is $N_y^{\text{PBK}} = N_x^{\text{PBK}}$.

Similarly, the perturbed current in the z -direction is given by

$$\begin{aligned}
\delta J_z^{\text{PBK}} = & i\epsilon_0 \sum_s \omega_{ps} \delta E_z + \sum_{sn} \sum_{l=1}^{\kappa_{\parallel s}-1} \frac{b_{z34sn,l+2}}{\omega(\omega - c_{sn})^l} \delta E_z, \\
& + \sum_{sn} \sum_{l=1}^{\kappa_{\parallel s}} \left[\frac{b_{z13sn,l+1}}{\omega(\omega - c_{sn})^l} \delta E_x + \frac{b_{z23sn,l+1}}{\omega(\omega - c_{sn})^l} \delta E_y + \frac{b_{z33sn,l+1}}{\omega(\omega - c_{sn})^l} \delta E_z \right] \\
& + \sum_{sn} \sum_{l=1}^{\kappa_{\parallel s}+1} \left[\frac{b_{z11snl}}{\omega(\omega - c_{sn})^l} \delta E_x + \frac{b_{z21snl}}{\omega(\omega - c_{sn})^l} \delta E_y + \frac{b_{z31snl}}{\omega(\omega - c_{sn})^l} \delta E_z \right] \\
& + \sum_{sn} \sum_{l=1}^{\kappa_{\parallel s}+1} \left[\frac{b_{z12snl}}{\omega(\omega - c_{sn})^{l+1}} \delta E_x + \frac{b_{z22snl}}{\omega(\omega - c_{sn})^{l+1}} \delta E_y + \frac{b_{z32snl}}{\omega(\omega - c_{sn})^{l+1}} \delta E_z \right], \tag{32}
\end{aligned}$$

where

$$\left\{ \begin{aligned}
b_{z10} &= -i\epsilon_0 \tan \theta \sum_s \omega_{ps}^2, & b_{z11snl} &= -i\epsilon_0 \tan \theta \omega_{ps}^2 n \left[\frac{(c_{sn} - n\omega_{cs}) b_{1snl} + b_{2snl}}{\omega_{cs}} \right], \\
b_{z30} &= i\epsilon_0 \tan^2 \theta \sum_s \omega_{ps}^2, & b_{z12snl} &= -i\epsilon_0 \tan \theta \omega_{ps}^2 n \left[\frac{(c_{sn} - n\omega_{cs}) b_{2snl}}{\omega_{cs}} \right], \\
b_{z13snl} &= -i\epsilon_0 \tan \theta \omega_{ps}^2 n \left(\frac{b_{1snl}}{\omega_{cs}} \right), & b_{z21snl} &= \epsilon_0 \tan \theta \omega_{ps}^2 \left[\frac{(c_{sn} - n\omega_{cs}) b_{3snl} + b_{4snl}}{\omega_{cs}} \right], \\
b_{z22snl} &= \epsilon_0 \tan \theta \omega_{ps}^2 \left[\frac{(c_{sn} - n\omega_{cs}) b_{4snl}}{\omega_{cs}} \right], & b_{z23snl} &= \epsilon_0 \tan \theta \omega_{ps}^2 \left(\frac{b_{3snl}}{\omega_{cs}} \right), \\
b_{z31snl} &= -i\epsilon_0 \tan^2 \theta \omega_{ps}^2 \left[\frac{(c_{sn} - n\omega_{cs})^2 b_{1snl} + 2(c_{sn} - n\omega_{cs}) b_{2snl}}{\omega_{cs}^2} \right], & & \\
b_{z32snl} &= -i\epsilon_0 \tan^2 \theta \omega_{ps}^2 \left[\frac{(c_{sn} - n\omega_{cs})^2 b_{2snl}}{\omega_{cs}^2} \right], & & \\
b_{z33snl} &= -i\epsilon_0 \tan^2 \theta \omega_{ps}^2 \left[\frac{2(c_{sn} - n\omega_{cs}) b_{1snl} + b_{2snl}}{\omega_{cs}^2} \right], & b_{z34snl} &= -i\epsilon_0 \tan^2 \theta \omega_{ps}^2 \left(\frac{b_{1snl}}{\omega_{cs}^2} \right), \\
\sum_{sn} b_{z13sn1} &= -b_{z10}, & \sum_{sn} b_{z23sn1} &= 0, & \sum_{sn} b_{z33sn1} &= i\epsilon_0 \sum_s \omega_{ps}^2, \\
\sum_{sn} c_{sn} b_{z34sn1} &= b_{z30}, & \sum_{sn} b_{z34sn2} &= 0, & \sum_{sn} b_{z34sn1} &= 0. \tag{33}
\end{aligned} \right.$$

Following the same methodology, Eq. (32) for z -direction yields the linear

system $\omega \mathbf{z} = \mathbf{M}_z \mathbf{z}$, the explicit form is given by

$$\left\{ \begin{array}{l} \omega \delta J_z^{\text{PBK}} = i\epsilon_0 \sum_s \omega_{ps}^2 \delta E_z + \sum_{sn} \sum_{l=1}^{\kappa_{\parallel s}+1} z_{snl1}, \\ \omega z_{snl1} = c_{sn} z_{snl1} + z_{snl2}, \\ \vdots \\ \omega z_{snl,l-1} = c_{sn} z_{snl,l-1} + z_{snll}, \\ \omega z_{snll} = \begin{cases} b_{z34sn,l+2} \delta E_z + b_{z13sn,l+1} \delta E_x + b_{z23sn,l+1} \delta E_y + b_{z33sn,l+1} \delta E_z \\ + b_{z11snl} \delta E_x + b_{z21snl} \delta E_y + b_{z31snl} \delta E_z + c_{sn} z_{snll} + z_{snl,l+1}, & (\text{if } l \leq \kappa_{\parallel s} - 1), \\ b_{z13sn,l+1} \delta E_x + b_{z23sn,l+1} \delta E_y + b_{z33sn,l+1} \delta E_z \\ + b_{z11snl} \delta E_x + b_{z21snl} \delta E_y + b_{z31snl} \delta E_z + c_{sn} z_{snll} + z_{snl,l+1}, & (\text{if } l = \kappa_{\parallel s}), \\ b_{z11snl} \delta E_x + b_{z21snl} \delta E_y + b_{z31snl} \delta E_z + c_{sn} z_{snll} + z_{snl,l+1}, & (\text{if } l = \kappa_{\parallel s} + 1), \end{cases} \\ \omega z_{snl,l+1} = b_{z12snl} \delta E_x + b_{z22snl} \delta E_y + b_{z32snl} \delta E_z + c_{sn} z_{snl,l+1}, \end{array} \right. \quad (34)$$

where $\mathbf{z} = [z_{snl1}, z_{snl2}, \dots, z_{snl,l+1}, \delta J_z^{\text{PBK}}]^T$, the total number of equations in linear system (34) is $N_z^{\text{PBK}} = N_x^{\text{PBK}}$.

The above derivation constructs the total linear system for PBK plasma by combining the component systems in the x -, y -, and z -directions, given by Eqs. (28), (31), and (34), respectively. The total dimension of this system is $N_{\text{PBK}} = 3N_x^{\text{PBK}}$. Furthermore, Eqs. (A.1) and (A.2) establish the equivalence between the component systems for the x - and z -directions (28) and (34), and their respective perturbed currents, (26) and (32).

3.2. Equivalent linear system for BM plasmas

The perturbed current in BM plasma is derived from equations (22) and (12) combined with Ohm's law (25), giving the simplified expressions [9, 20],

$$\begin{pmatrix} \delta J_x^{\text{BM}} \\ \delta J_y^{\text{BM}} \\ \delta J_z^{\text{BM}} \end{pmatrix} = \begin{pmatrix} \frac{b_{x1}^{\text{BM}}}{\omega} + \sum_{snj} \frac{b_{x1snj}^{\text{BM}}}{\omega - \bar{c}_{snj}} & \frac{b_{x2}^{\text{BM}}}{\omega} + \sum_{snj} \frac{b_{x2snj}^{\text{BM}}}{\omega - \bar{c}_{snj}} & \frac{b_{x3}^{\text{BM}}}{\omega} + \sum_{snj} \frac{b_{x3snj}^{\text{BM}}}{\omega - \bar{c}_{snj}} \\ \frac{b_{y1}^{\text{BM}}}{\omega} + \sum_{snj} \frac{b_{y1snj}^{\text{BM}}}{\omega - \bar{c}_{snj}} & \frac{b_{y2}^{\text{BM}}}{\omega} + \sum_{snj} \frac{b_{y2snj}^{\text{BM}}}{\omega - \bar{c}_{snj}} & \frac{b_{y3}^{\text{BM}}}{\omega} + \sum_{snj} \frac{b_{y3snj}^{\text{BM}}}{\omega - \bar{c}_{snj}} \\ \frac{b_{z1}^{\text{BM}}}{\omega} + \sum_{snj} \frac{b_{z1snj}^{\text{BM}}}{\omega - \bar{c}_{snj}} & \frac{b_{z2}^{\text{BM}}}{\omega} + \sum_{snj} \frac{b_{z2snj}^{\text{BM}}}{\omega - \bar{c}_{snj}} & \frac{b_{z3}^{\text{BM}}}{\omega} + \sum_{snj} \frac{b_{z3snj}^{\text{BM}}}{\omega - \bar{c}_{snj}} \end{pmatrix} \begin{pmatrix} \delta E_x \\ \delta E_y \\ \delta E_z \end{pmatrix}, \quad (35)$$

where

$$\left\{ \begin{array}{l} b_{x1}^{\text{BM}} = i\epsilon_0 \left(\sum_s \omega_{ps}^2 + \sum_{snj} \omega_{ps}^2 n^2 \frac{\tilde{b}_{12snj}}{\tilde{c}_{snj}} \right), \quad b_{x2}^{\text{BM}} = -\epsilon_0 \sum_{snj} \omega_{ps}^2 n^2 \frac{\tilde{b}_{34snj}}{\tilde{c}_{snj}}, \\ b_{x3}^{\text{BM}} = -i\epsilon_0 \tan \theta \left(\sum_s \omega_{ps}^2 + \sum_{snj} \omega_{ps}^2 n^2 \frac{\tilde{b}_{12snj}}{\tilde{c}_{snj}} \right), \quad b_{x1snj}^{\text{BM}} = -i\epsilon_0 \omega_{ps}^2 n^2 \frac{\tilde{b}_{12snj}}{\tilde{c}_{snj}}, \\ b_{x2snj}^{\text{BM}} = \epsilon_0 \omega_{ps}^2 n^2 \frac{\tilde{b}_{34snj}}{\tilde{c}_{snj}}, \quad b_{x3snj}^{\text{BM}} = -i\epsilon_0 \tan \theta \omega_{ps}^2 n^2 \frac{(1-n\omega_{cs}/\tilde{c}_{snj})\tilde{b}_{12snj}}{\omega_{cs}}, \\ b_{y1}^{\text{BM}} = \epsilon_0 \sum_{snj} \omega_{ps}^2 n^2 \frac{\tilde{b}_{34snj}}{\tilde{c}_{snj}}, \quad b_{y2}^{\text{BM}} = i\epsilon_0 \left(\sum_s \omega_{ps}^2 + \sum_{snj} \omega_{ps}^2 n^2 \frac{\tilde{b}_{56snj}}{\tilde{c}_{snj}} \right), \\ b_{y3}^{\text{BM}} = -\epsilon_0 \tan \theta \sum_{snj} \omega_{ps}^2 n^2 \frac{\tilde{b}_{34snj}}{\tilde{c}_{snj}}, \quad b_{y1snj}^{\text{BM}} = -\epsilon_0 \omega_{ps}^2 n^2 \frac{\tilde{b}_{34snj}}{\tilde{c}_{snj}}, \\ b_{y2snj}^{\text{BM}} = -i\epsilon_0 \omega_{ps}^2 n^2 \frac{\tilde{b}_{56snj}}{\tilde{c}_{snj}}, \quad b_{y3snj}^{\text{BM}} = -\epsilon_0 \tan \theta \omega_{ps}^2 n^2 \frac{(1-n\omega_{cs}/\tilde{c}_{snj})\tilde{b}_{34snj}}{\omega_{cs}}, \\ b_{z1}^{\text{BM}} = -i\epsilon_0 \tan \theta \left(\sum_s \omega_{ps}^2 + \sum_{snj} \omega_{ps}^2 n^2 \frac{\tilde{b}_{12snj}}{\tilde{c}_{snj}} \right), \quad b_{z2}^{\text{BM}} = \epsilon_0 \tan \theta \sum_{snj} \omega_{ps}^2 n^2 \frac{\tilde{b}_{34snj}}{\tilde{c}_{snj}}, \\ b_{z3}^{\text{BM}} = i\epsilon_0 \tan^2 \theta \left(\sum_s \omega_{ps}^2 + \sum_{snj} \omega_{ps}^2 n^2 \frac{\tilde{b}_{12snj}}{\tilde{c}_{snj}} \right), \quad b_{z1snj}^{\text{BM}} = -i\epsilon_0 \tan \theta \omega_{ps}^2 n^2 \frac{(1-n\omega_{cs}/\tilde{c}_{snj})\tilde{b}_{12snj}}{\omega_{cs}}, \\ b_{z2snj}^{\text{BM}} = \epsilon_0 \tan \theta \omega_{ps}^2 n^2 \frac{(1-n\omega_{cs}/\tilde{c}_{snj})\tilde{b}_{34snj}}{\omega_{cs}}, \quad b_{z3snj}^{\text{BM}} = -i\epsilon_0 \tan^2 \theta \omega_{ps}^2 \tilde{b}_{12snj} \left(\frac{\tilde{c}_{snj}}{\omega_{cs}^2} - \frac{2n}{\omega_{cs}} + \frac{n^2}{\tilde{c}_{snj}} \right). \end{array} \right. \quad (36)$$

The three perturbed currents in Eq. (35) form a linear subsystem given by

$$\left\{ \begin{array}{l} \omega \delta J_{x1}^{\text{BM}} = b_{x1}^{\text{BM}} \delta E_x + b_{x2}^{\text{BM}} \delta E_y + b_{x3}^{\text{BM}} \delta E_z, \\ \omega \delta J_{x2}^{\text{BM}} = \omega \sum_{snj} \tilde{x}_{snj} = \sum_{snj} \tilde{c}_{snj} \tilde{x}_{snj} + \sum_{snj} b_{x1snj}^{\text{BM}} \delta E_x + \sum_{snj} b_{x2snj}^{\text{BM}} \delta E_y + \sum_{snj} b_{x3snj}^{\text{BM}} \delta E_z, \\ \omega \tilde{x}_{snj} = \tilde{c}_{snj} \tilde{x}_{snj} + b_{x1snj}^{\text{BM}} \delta E_x + b_{x2snj}^{\text{BM}} \delta E_y + b_{x3snj}^{\text{BM}} \delta E_z, \end{array} \right. \quad (37)$$

$$\left\{ \begin{array}{l} \omega \delta J_{y1}^{\text{BM}} = b_{y1}^{\text{BM}} \delta E_x + b_{y2}^{\text{BM}} \delta E_y + b_{y3}^{\text{BM}} \delta E_z, \\ \omega \delta J_{y2}^{\text{BM}} = \omega \sum_{snj} \tilde{y}_{snj} = \sum_{snj} \tilde{c}_{snj} \tilde{y}_{snj} + \sum_{snj} b_{y1snj}^{\text{BM}} \delta E_x + \sum_{snj} b_{y2snj}^{\text{BM}} \delta E_y + \sum_{snj} b_{y3snj}^{\text{BM}} \delta E_z, \\ \omega \tilde{y}_{snj} = \tilde{c}_{snj} \tilde{y}_{snj} + b_{y1snj}^{\text{BM}} \delta E_x + b_{y2snj}^{\text{BM}} \delta E_y + b_{y3snj}^{\text{BM}} \delta E_z, \end{array} \right. \quad (38)$$

and

$$\left\{ \begin{array}{l} \omega \delta J_{z1}^{\text{BM}} = b_{z1}^{\text{BM}} \delta E_x + b_{z2}^{\text{BM}} \delta E_y + b_{z3}^{\text{BM}} \delta E_z, \\ \omega \delta J_{z2}^{\text{BM}} = \omega \sum_{snj} \tilde{z}_{snj} = \sum_{snj} \tilde{c}_{snj} \tilde{z}_{snj} + \sum_{snj} b_{z1snj}^{\text{BM}} \delta E_x + \sum_{snj} b_{z2snj}^{\text{BM}} \delta E_y + \sum_{snj} b_{z3snj}^{\text{BM}} \delta E_z, \\ \omega \tilde{z}_{snj} = \tilde{c}_{snj} \tilde{z}_{snj} + b_{z1snj}^{\text{BM}} \delta E_x + b_{z2snj}^{\text{BM}} \delta E_y + b_{z3snj}^{\text{BM}} \delta E_z. \end{array} \right. \quad (39)$$

Here, the perturbed currents are defined as $\delta J_x^{\text{BM}} = \delta J_{x1}^{\text{BM}} + \delta J_{x2}^{\text{BM}}$, $\delta J_y^{\text{BM}} = \delta J_{y1}^{\text{BM}} + \delta J_{y2}^{\text{BM}}$, $\delta J_z^{\text{BM}} = \delta J_{z1}^{\text{BM}} + \delta J_{z2}^{\text{BM}}$, with the summation operator $\sum_{snj} = \sum_{s=1}^{S_{\text{BM}}} \sum_{n=-N_s}^{N_s} \sum_{j=1}^J$. Each eigenvalue subsystem, for the x -, y -, or z -direction, consists of the corresponding equations (37), (38), and (39) and contains of $N_x^{\text{BM}} = N_y^{\text{BM}} = N_z^{\text{BM}} = 2 + \sum_1^{S_{\text{BM}}} \sum_{n=-N_s}^{N_s} J$ equations. Consequently, the total dimension of the linear system for the BM plasma is $N_{\text{BM}} = 3N_x^{\text{BM}}$.

3.3. Equivalent closed linear system

The complete PBK-BM linear system combines the PBK system (Eqs. (28), (31), and (34)), the BM system (Eqs. (37), (38), and (39)), and Maxwell's equations in their perturbed component form

$$\omega\delta E_x = c^2 k_z \delta B_y - i \frac{\delta J_x}{\epsilon_0}, \quad (40a)$$

$$\omega\delta E_y = -c^2 k_z \delta B_x + c^2 k_x \delta B_z - i \frac{\delta J_y}{\epsilon_0}, \quad (40b)$$

$$\omega\delta E_z = -c^2 k_x \delta B_y - i \frac{\delta J_z}{\epsilon_0}, \quad (40c)$$

$$\omega\delta B_x = -k_z \delta E_y, \quad (40d)$$

$$\omega\delta B_y = k_z \delta E_x - k_x \delta E_z, \quad (40e)$$

$$\omega\delta B_z = k_x \delta E_y. \quad (40f)$$

The perturbed currents in Eqs. (40a), (40b), and (40c) arise from both the PBK and BM plasmas, and are decomposed into distinct components as follows: $\delta J_x = \delta J_x^{\text{PBK}} + \delta J_{x1}^{\text{BM}} + \delta J_{x2}^{\text{BM}}$, $\delta J_y = \delta J_y^{\text{PBK}} + \delta J_{y1}^{\text{BM}} + \delta J_{y2}^{\text{BM}}$, and $\delta J_z = \delta J_z^{\text{PBK}} + \delta J_{z1}^{\text{BM}} + \delta J_{z2}^{\text{BM}}$. The resulting closed PBK-BM linear system governing oblique electromagnetic wave propagation is given by $\omega\mathbf{x} = \mathbf{Bx}$. The vector is $\mathbf{x} = [\mathbf{x}_{\text{PBK}}, \mathbf{x}_{\text{BM}}, \delta\mathbf{J}_1^{\text{BM}}, \delta\mathbf{E}, \delta\mathbf{B}]^T$, and the matrix \mathbf{B} is defined as follows

$$\mathbf{B} = [\mathbf{B}_{\text{PBK}}, \mathbf{B}_{\text{BM}}, \mathbf{B}_{\text{Maxwell}}]^T, \quad (41)$$

where

$$\mathbf{x}_{\text{PBK}} = \left[\underbrace{x_{snl1}, \dots, x_{snl,l+1}, \delta J_x^{\text{PBK}}}_{N_x^{\text{PBK}}}, \dots, \underbrace{z_{snl1}, \dots, z_{snl,l+1}, \delta J_z^{\text{PBK}}}_{N_z^{\text{PBK}}} \right], \quad (42a)$$

$$\mathbf{x}_{\text{BM}} = \left[\underbrace{\tilde{x}_{snj}, \delta J_{x2}^{\text{BM}}}_{N_x^{\text{BM}}}, \dots, \underbrace{\tilde{z}_{snj}, \delta J_{z2}^{\text{BM}}}_{N_z^{\text{BM}}} \right], \quad \delta\mathbf{J}_1^{\text{BM}} = [\delta J_{x1}^{\text{BM}}, \delta J_{y1}^{\text{BM}}, \delta J_{z1}^{\text{BM}}], \quad (42b)$$

$$\delta\mathbf{E} = [\delta E_x, \delta E_y, \delta E_z], \quad \delta\mathbf{B} = [\delta B_x, \delta B_y, \delta B_z]. \quad (42c)$$

The complete linear system for the plasma comprising PBK and BM components is represented by a sparse matrix of order N^{closed} , where $N^{\text{closed}} =$

$N_{\text{PBK}} + N_{\text{BM}} + 6$ denotes the total number of degrees of freedom. This global system matrix \mathbf{B} is assembled from the following submatrices: the PBK plasma submatrix \mathbf{B}_{PBK} , of dimension $N_{\text{PBK}} \times N^{\text{closed}}$, defined by Eqs. (28), (31), and (34); the BM plasma submatrix \mathbf{B}_{BM} , of dimension $N_{\text{BM}} \times N^{\text{closed}}$, defined by Eqs. (37), (38), and (39); and the Maxwell submatrix $\mathbf{B}_{\text{Maxwell}}$, of dimension $6 \times N^{\text{closed}}$, determined by the Maxwell component equation set (40). For the independent PBK or BM plasma models, the corresponding closed linear systems are described by sparse matrices of orders $N_{\text{PBK}}^{\text{closed}} = N_{\text{PBK}} + 6$ and $N_{\text{BM}}^{\text{closed}} = N_{\text{BM}} + 6$, respectively. By setting $\kappa_{\perp s}$ to a sufficiently large value (e.g., 200) in the BO-PBK solver, we force the PBK plasma model to converge to the KM plasma, which numerically represents the Maxwellian limit ($\kappa_{\perp s} \rightarrow \infty$). The computational efficiency of the BO-PBK solver is highly sensitive to $\kappa_{\parallel s}$ index, as high values cause a prohibitive increase in matrix dimension. For instance, in the BO-PBK solver with $N = 10$ and $S = 1$, increasing κ_{\parallel} from 2 to 14 raises $N_{\text{PBK}}^{\text{closed}}$ from 576 to 8514, while the resulting matrix dimensions remain only about one-half to one-third of those required by the BO-KM solver [15]. When $\kappa_{\parallel s}$ is large, the distribution approaches a Maxwellian. For computational convenience, the algorithm switches to the BM matrix for the s th species eigenvalue problem whenever $\kappa_{\parallel s}$ exceeds the threshold $\kappa_{\parallel s,th}$.

4. Benchmarks and applications

In this section, we report the results of applying the BO-PBK solver to several representative test cases to validate its performance. These cases were computed on a system equipped with an Intel Core i7-8850H CPU, using MATLAB's eigenvalue functions `eig()` or `eigs()` for solution.

Case 1: R-, L-, and P-mode waves

On the electron time scale, four modes are identified within the ω_{ce} range: the off-parallel L-X wave (left-hand circularly polarized), the upper and lower branches of the R-X wave (right-hand circularly polarized), and the O-P wave (ordinary plasma wave). At a fixed angle of $\theta = 30^\circ$, our numerical results (Fig. 3) show excellent agreement with Ref. [13].

Case 2: Whistler instability

The electron whistler instability is highly sensitive to anisotropic distribution shapes, making it ideal for BO-PBK solver validation. We compare

with the weakly magnetized plasma ($|\omega_{ce}|/\omega_{pe} = 0.01$) studied by Lazar et al. [1], which consists electrons (e) and protons (p) with $T_{\perp(e,p)}/T_{\parallel(e,p)} = 4$. Figure 4 shows the real frequencies and growth rates of parallel electron whistler-cyclotron modes for PBK plasma ($\kappa_{\parallel,\perp(e,p)} = 2, 6$) and BM plasma. The BO-PBK results (colored solid lines) agree well with the reference data (black dashed lines) from [1].

We also benchmark the BO-PBK solver using electron whistlers in moderately magnetized plasmas ($|\omega_{ce}|/\omega_{pe} = 0.5$) from Cattaert et al. [13]. Figure 5 shows the dispersion relation and damping/growth rates under different electron temperature anisotropies.

Case 3: Firehose instability

We benchmark the BO-PBK code against the parallel (PFHI) and oblique (OFHI) firehose instability cases from the LEOPARD code [22]. The thermal plasma consists of electrons and ions with following parameters[26, 15]: electrons have an isotropic BM distribution with $\beta_e = 1$, while ions follow an anisotropic distribution (BM or KM) with $\beta_{\parallel i} = 4$ and $\beta_{\perp i} = 2$. Figure 6 compares BO-PBK results with Ref. [26]. The ion inertial length is $d_i = v_A/\omega_{ci}$, where the Alfvén velocity is $v_A = B_0/\sqrt{\mu_0 m_i n_i}$. Figure 7 shows OFHI ($\theta = 45^\circ$) computed by the BO-PBK solver under the same parameters for different ion distributions: BM, KM($\kappa_{\parallel i} = 2, 4, 8, \kappa_{\perp i} = 200$), and PBK($\kappa_{\parallel i} = 2, 4, 8, \kappa_{\perp i} = 10$). Figure 8 presents contour plots of the PFHI and OFHI for ions with BM (a) and PBK (b) distributions at various propagation angles.

Case 4: Ion cyclotron instability

The current-driven ion cyclotron instability plays a critical role in plasma heating processes in both space and laboratory plasmas. We benchmark the BO-PBK solver against the computational results of Basu [34]. Figures 9 and 10 show the spectral behavior (ω_r and ω_i versus k_\perp at $k_\parallel/(\sqrt{2}\rho_i) = 0.08$) of the unstable ion-cyclotron modes for selected $T_{\parallel e}/T_{\perp i}$ and $T_{\parallel i}/T_{\perp i}$ values. Figure 11 compares the growth rates from the BM and PBK models for different ion loss-cone parameters ($\sigma_i = 0, 0.5, 1$) at $T_{\parallel i}/T_{\perp i} = 5$, The results demonstrate that the ion loss-cone reduces the growth rate of in this mode.

To further validate the BO-PBK solver, we examine electromagnetic ion cyclotron (EMIC) waves driven by temperature-anisotropic superthermal protons in a multi-particle plasma composed of cold H^+ , He^+ , and O^+ ions [25]. Using plasma parameters from Refs. [25, 15], we compute the

dispersion relations and the growth rates of the H^+ -band (dominant) and He^+ -band (subdominant) EMIC instabilities for oblique propagation angles $\theta = 0^\circ, 15^\circ, 40^\circ, 55^\circ$ (Figs. 12(a)-(d)). The BO-PBK solver results (colored solid curves) for superthermal protons with a KM distribution ($\kappa_{\parallel p} = 1$ and $\kappa_{\perp p} = 200$), show excellent agreement with the BO-KM benchmarks [15] (black dashed lines). With parameters ($S = 4$, $J = 8$, and $N = 1$) identical to the BO-KM solver [15], computing all 100 wave vector points and 60 angle points takes approximately 76 minutes of CPU time, which is only about 40% of that required by BO-KM. The efficiency advantage of BO-PBK over BO-KM becomes even more pronounced for large values of $\kappa_{\parallel s}$.

5. Summary and discussion

This paper presents an enhanced BO-PBK solver for analyzing waves and instabilities in magnetized multi-component plasmas with non-Maxwellian, anisotropic features like power-law tails. The solver models plasmas as temperature-anisotropic conductive media within a unified framework. By linearizing the Vlasov-Maxwell equations with rational dispersion functions ($\mathcal{Z}_{\kappa_{\parallel s}}$ and Z_J), it constructs a concise, self-consistent linear system, thereby casting the dispersion relation as a standard eigenvalue problem. This enables the solver to handle a wide range of velocity distributions, including anisotropic, loss-cone, drift PBK, KM, BM, and hybrid models.

In BO-PBK solver, adapts to different plasma regimes based on key parameters: the s th component approximates a KM plasma for large $\kappa_{\perp s}$, and is treated as BM plasma when $\kappa_{\parallel s}$ exceeds a predefined threshold $\kappa_{\parallel s}^{\text{threshold}}$. User-defined simulations are configured via the `bopbk.in` input file. The solver's performance was evaluated against benchmark cases involving waves and instabilities from distributions, including drift, temperature-anisotropic, and multi-component hybrid distributions. The excellent agreement of the numerical results with established references [1, 13, 25, 15] validates the effectiveness and accuracy of the new BO-PBK solver.

In summary, the BO-PBK solver efficiently computes multiple eigenroots of the dispersion relation for obliquely propagating waves in magnetized plasmas featuring high-energy tail distributions. It resolves multiple key plasma wave and instability modes simultaneously, eliminating the need for iterative initial-value searches. The solver is uniformly applicable to hybrid distribution models, such as PBK, KM, and BM, making it well-suited for analyzing dispersion properties and instabilities in both space and laboratory plasmas.

Compared to the BO-KM solver, the present method extends applicability to loss-cone and PBK plasmas and reduces the PBK linear system to three sub-matrices (\mathbf{M}_x , \mathbf{M}_y , and \mathbf{M}_z). Moreover, the proposed transformation method also generalizes to eigenvalue problems arising from dispersion relations in plasmas with arbitrary velocity distributions. Future work will be report related advances.

The source code for this work is available at <https://github.com/baiweiphys/BOPBK>.

Acknowledgments

We are grateful to Jinsong Zhao and Yu Liu for their insightful discussions and valuable suggestions on this research.

Appendix A. Proof of the equivalence of linear subsystems

From (28), we have

$$\begin{aligned}
\delta J_x^{\text{PBK}} &= \frac{b_{x10}}{\omega} \delta E_x + \sum_{sn} \sum_{l=1}^{\kappa_{\parallel s}+1} \frac{x_{snl1}}{\omega} = \frac{b_{x10}}{\omega} \delta E_x + \sum_{sn} \sum_{l=1}^{\kappa_{\parallel s}+1} \frac{x_{snl2}}{\omega(\omega - c_{sn})} \\
&= \dots = \frac{b_{x10}}{\omega} \delta E_x + \sum_{sn} \sum_{l=1}^{\kappa_{\parallel s}+1} \frac{x_{snll}}{\omega(\omega - c_{sn})^{l-1}} \\
&= \frac{b_{x10}}{\omega} \delta E_x + \sum_{sn} \sum_{l=1}^{\kappa_{\parallel s}} \frac{b_{x33snl,l+1}}{\omega(\omega - c_{sn})^l} \delta E_z \\
&\quad + \sum_{sn} \sum_{l=1}^{\kappa_{\parallel s}+1} \left[\frac{b_{x11snl}\delta E_x}{\omega(\omega - c_{sn})^l} + \frac{b_{x21snl}\delta E_y}{\omega(\omega - c_{sn})^l} + \frac{b_{x31snl}\delta E_z}{\omega(\omega - c_{sn})^l} + \frac{x_{snl,l+1}}{\omega(\omega - c_{sn})^l} \right] \text{A.1)} \\
&= \frac{b_{x10}}{\omega} \delta E_x + \sum_{sn} \sum_{l=1}^{\kappa_{\parallel s}} \frac{b_{x33snl}}{\omega(\omega - c_{sn})^{l-1}} \delta E_z \\
&\quad + \sum_{sn} \sum_{l=1}^{\kappa_{\parallel s}+1} \left[\frac{b_{x11snl}\delta E_x}{\omega(\omega - c_{sn})^l} + \frac{b_{x21snl}\delta E_y}{\omega(\omega - c_{sn})^l} + \frac{b_{x31snl}\delta E_z}{\omega(\omega - c_{sn})^l} \right] \\
&\quad + \sum_{sn} \sum_{l=1}^{\kappa_{\parallel s}+1} \left[\frac{b_{x12snl}\delta E_x}{\omega(\omega - c_{sn})^{l+1}} + \frac{b_{x22snl}\delta E_y}{\omega(\omega - c_{sn})^{l+1}} + \frac{b_{x32snl}\delta E_z}{\omega(\omega - c_{sn})^{l+1}} \right].
\end{aligned}$$

Similarly, from (34), we obtain,

$$\begin{aligned}
\delta J_z^{\text{PBK}} &= i\epsilon_0 \sum_s \omega_{ps}^2 \delta E_z + \sum_{sn} \sum_{l=1}^{\kappa_{\parallel s}+1} \frac{z_{snl1}}{\omega} = i\epsilon_0 \sum_s \omega_{ps}^2 \delta E_z + \sum_{sn} \sum_{l=1}^{\kappa_{\parallel s}+1} \frac{z_{snl2}}{\omega(\omega - c_{sn})} \\
&= \dots = i\epsilon_0 \sum_s \omega_{ps}^2 \delta E_z + \sum_{sn} \sum_{l=1}^{\kappa_{\parallel s}+1} \frac{z_{snl2}}{\omega(\omega - c_{sn})^{l-1}} \\
&= i\epsilon_0 \sum_s \omega_{ps}^2 \delta E_z + \sum_{sn} \sum_{l=1}^{\kappa_{\parallel s}-1} \frac{b_{z34sn,l+2}}{\omega(\omega - c_{sn})^l} \delta E_z \\
&\quad + \sum_{sn} \sum_{l=1}^{\kappa_{\parallel s}} \left[\frac{b_{z13sn,l+1}\delta E_x}{\omega(\omega - c_{sn})^l} + \frac{b_{z23sn,l+1}\delta E_y}{\omega(\omega - c_{sn})^l} + \frac{b_{z33sn,l+1}\delta E_z}{\omega(\omega - c_{sn})^l} \right] \\
&\quad + \sum_{sn} \sum_{l=1}^{\kappa_{\parallel s}+1} \left[\frac{b_{z11snl}\delta E_x}{\omega(\omega - c_{sn})^l} + \frac{b_{z21snl}\delta E_y}{\omega(\omega - c_{sn})^l} + \frac{b_{z31snl}\delta E_z}{\omega(\omega - c_{sn})^l} + \frac{z_{snl,l+1}}{\omega(\omega - c_{sn})^l} \right] \text{A.2)} \\
&= i\epsilon_0 \sum_s \omega_{ps}^2 \delta E_z + \sum_{sn} \sum_{l=1}^{\kappa_{\parallel s}-1} \frac{b_{z34sn,l+2}}{\omega(\omega - c_{sn})^{l-1}} \delta E_z \\
&\quad + \sum_{sn} \sum_{l=1}^{\kappa_{\parallel s}} \left[\frac{b_{z13sn,l+1}\delta E_x}{\omega(\omega - c_{sn})^l} + \frac{b_{z23sn,l+1}\delta E_y}{\omega(\omega - c_{sn})^l} + \frac{b_{z33sn,l+1}\delta E_z}{\omega(\omega - c_{sn})^l} \right] \\
&\quad + \sum_{sn} \sum_{l=1}^{\kappa_{\parallel s}+1} \left[\frac{b_{z11snl}\delta E_x}{\omega(\omega - c_{sn})^l} + \frac{b_{z21snl}\delta E_y}{\omega(\omega - c_{sn})^l} + \frac{b_{z31snl}\delta E_z}{\omega(\omega - c_{sn})^l} \right] \\
&\quad + \sum_{sn} \sum_{l=1}^{\kappa_{\parallel s}+1} \left[\frac{b_{z12snl}\delta E_x}{\omega(\omega - c_{sn})^{l+1}} + \frac{b_{z22snl}\delta E_y}{\omega(\omega - c_{sn})^{l+1}} + \frac{b_{z32snl}\delta E_z}{\omega(\omega - c_{sn})^{l+1}} \right].
\end{aligned}$$

Appendix B. Useful formulas

(a) Limit formulas

$$\lim_{\kappa \rightarrow \infty} \left(1 + \frac{y^2}{\kappa} \right)^{-\kappa} = e^{-y^2}, \quad \lim_{n \rightarrow \infty} \frac{\Gamma(n+z)}{\Gamma(n)n^z} = 1. \quad (\text{B.1})$$

(b) Gamma function

$$\Gamma(z+1) = z\Gamma(z), \quad \Gamma(n) = (n-1)!, \quad \Gamma(n + \frac{1}{2}) = \sqrt{\pi} \frac{(2n)!}{4^n n!}. \quad (\text{B.2})$$

(c) Summation formulas for Bessel function [30]

$$\begin{cases} \sum_{n=-\infty}^{\infty} n J_n^2 = 0, \quad \sum_{n=-\infty}^{\infty} J_n J'_n = 0, \quad \sum_{n=-\infty}^{\infty} J_n^2 = 1, \\ \sum_{n=-\infty}^{\infty} (J'_n)^2 = \frac{1}{2}, \quad \sum_{n=-\infty}^{\infty} n^2 J_n^2(z) = \frac{1}{2} z^2, \quad \sum_{n=-\infty}^{\infty} n J_n J'_n = 0, \\ \sum_{n=-\infty}^{\infty} I_n(z) = \sum_{n=-\infty}^{\infty} I'_n(z) = \exp(z), \quad \sum_{n=-\infty}^{\infty} n^2 I_n(z) = z \exp(z), \\ \sum_{n=-\infty}^{\infty} n I_n = \sum_{n=-\infty}^{\infty} n I'_n = 0. \end{cases} \quad (\text{B.3})$$

(d) Gamma function Integrals

$$\int_0^{\infty} \frac{x^{\mu-1}}{(p+qx^2)^{\nu}} dx = \frac{\Gamma(\mu/2)\Gamma(\nu-\mu/2)}{2\Gamma(\nu)} \frac{1}{q^{\mu/2}} \frac{1}{p^{(\nu-\mu/2)}}, \quad (\text{B.4a})$$

$$\int_0^{\infty} x^{\mu-1} e^{-\nu x^2} dx = \frac{\Gamma(\mu/2)}{2\nu^{\mu/2}}. \quad (\text{B.4b})$$

(e) Integrals involving modified Bessel functions

$$\begin{cases} \int_0^{\infty} x J_n^2(x) \exp\left(-\frac{x^2}{2\lambda}\right) dx = \lambda \Lambda_n, \\ \int_0^{\infty} x^2 J_n(x) J'_n(x) \exp\left(-\frac{x^2}{2\lambda}\right) dx = \lambda^2 \Lambda'_n, \\ \int_0^{\infty} x^3 J_n^{2\prime}(x) \exp\left(-\frac{x^2}{2\lambda}\right) dx = n^2 \lambda \Lambda_n - 2\lambda^3 \Lambda'_n, \end{cases} \quad (\text{B.5})$$

where $\lambda > 0$; $n = 0, \pm 1, \pm 2, \dots$. Here, Λ_n and its derivative are given by

$$\Lambda_n = I_n(\lambda) e^{-\lambda}, \quad \Lambda'_n = I'_n(\lambda) e^{-\lambda} - I_n(\lambda) e^{-\lambda}. \quad (\text{B.6})$$

where I_n is the modified Bessel function of the first kind of order n , whose derivative obeys

$$I'_n(\lambda) = \frac{1}{2} [I_{n-1}(\lambda) + I_{n+1}(\lambda)]. \quad (\text{B.7})$$

References

- [1] M. LAZAR, S. POEDTS, and R. SCHLICKEISER, “Instability of the parallel electromagnetic modes in Kappa distributed plasmas – I. Electron whistler-cyclotron modes,” *Monthly Notices of the Royal Astronomical Society*, **410**, 1, 663 (2010).
- [2] M. LAZAR, R. SCHLICKEISER, and S. POEDTS, “Suprathermal Particle Populations in the Solar Wind and Corona,” in *Exploring the Solar Wind*, edited by M. LAZAR, chapter 11, IntechOpen, Rijeka, 2012.

- [3] M. MAKSIMOVIC, A. P. WALSH, V. PIERRARD, Š. ŠTVERÁK, and I. ZOUGANELIS, “Electron Kappa Distributions in the Solar Wind: Cause of the Acceleration or Consequence of the Expansion?,” in *Kappa Distributions: From Observational Evidences via Controversial Predictions to a Consistent Theory of Nonequilibrium Plasmas*, edited by M. LAZAR and H. FICHTNER, p. 39–51, Springer International Publishing, Cham, 2021.
- [4] M. LAZAR, R. A. LÓPEZ, S. POEDTS, and S. M. SHAABAN, “Instability of Langmuir-beam waves: Kappa-distributed electrons,” *Physics of Plasmas*, **30**, 8, 082106 (2023).
- [5] G. NICOLAOU, G. LIVADIOTIS, and R. T. WICKS, “On the Determination of Kappa Distribution Functions from Space Plasma Observations,” *Entropy*, **22**, 2 (2020).
- [6] D. SUMMERS and R. M. THORNE, “The modified plasma dispersion function,” *Physics of Fluids B: Plasma Physics*, **3**, 8, 1835 (1991).
- [7] D. SUMMERS, S. XUE, and R. M. THORNE, “Calculation of the dielectric tensor for a generalized Lorentzian (kappa) distribution function,” *Physics of Plasmas*, **1**, 6, 2012 (1994).
- [8] A. SHRAUNER and W. C. FELDMAN, “Electromagnetic ion-cyclotron wave growth rates and their variation with velocity distribution function shape,” *Journal of Plasma Physics*, **17**, 1, 123131 (1977).
- [9] W. BAI et al., “A new generalized formulation of dielectric tensor for multi-species plasma with anisotropic drift product-bi-kappa distribution,” *Physics of Plasmas*, **31**, 12, 122901 (2024).
- [10] D. SUMMERS and S. STONE, “The subtracted-kappa distribution and its properties,” *Physics of Plasmas*, **32**, 1, 012112 (2025).
- [11] R. L. MACE and M. A. HELLBERG, “A dispersion function for plasmas containing superthermal particles,” *Physics of Plasmas*, **2**, 6, 2098 (1995).
- [12] M. A. HELLBERG and R. L. MACE, “Generalized plasma dispersion function for a plasma with a kappa-Maxwellian velocity distribution,” *Physics of Plasmas*, **9**, 5, 1495 (2002).

- [13] T. CATTAERT, M. A. HELLBERG, and R. L. MACE, “Oblique propagation of electromagnetic waves in a kappa-Maxwellian plasma,” *Physics of Plasmas*, **14**, 8, 082111 (2007).
- [14] R. P. SINGHAL and A. K. TRIPATHI, “Dielectric tensor for a plasma with a loss-cone kappa-Maxwellian velocity distribution,” *Physics of Plasmas*, **13**, 1, 012102 (2006).
- [15] W. BAI, H. XIE, C. WU, Y. PU, and P. YU, “BO-KM: A comprehensive solver for dispersion relation of obliquely propagating waves in magnetized multi-species plasma with anisotropic drift kappa-Maxwellian distribution,” *Computer Physics Communications*, **307**, 109434 (2025).
- [16] K. Roennmark, “Waves in homogeneous, anisotropic multicomponent plasmas (WHAMP),” 1982.
- [17] A. F. VIÑAS, H. K. WONG, and A. J. KLIMAS, “Generation of Electron Suprathermal Tails in the Upper Solar Atmosphere: Implications for Coronal Heating,” *The Astrophysical Journal*, **528**, 1, 509 (2000).
- [18] K. G. KLEIN and G. G. HOWES, “Predicted impacts of proton temperature anisotropy on solar wind turbulence,” *Physics of Plasmas*, **22**, 3, 032903 (2015).
- [19] D. VERSCHAREN and B. D. G. CHANDRAN, “NHDS: The New Hampshire Dispersion Relation Solver,” *Research Notes of the AAS*, **2**, 2, 13 (2018).
- [20] H. XIE and Y. XIAO, “PDRK: A General Kinetic Dispersion Relation Solver for Magnetized Plasma,” *Plasma Science and Technology*, **18**, 2, 97 (2016).
- [21] H. SHENG XIE, “BO: A unified tool for plasma waves and instabilities analysis,” *Computer Physics Communications*, **244**, 343 (2019).
- [22] P. ASTFALK, T. GöRLER, and F. JENKO, “DSHARK: A dispersion relation solver for obliquely propagating waves in bi-kappa-distributed plasmas,” *Journal of Geophysical Research: Space Physics*, **120**, 9, 7107 (2015).

- [23] R. LÓPEZ, S. SHAABAN, and M. LAZAR, “General dispersion properties of magnetized plasmas with drifting bi-Kappa distributions. DIS-K: Dispersion Solver for Kappa Plasmas,” *Journal of Plasma Physics*, **87**, 3, 905870310 (2021).
- [24] W. BAI and H. XIE, “Toward developing a comprehensive algorithm for solving kinetic plasma dispersion relations for parallel propagation with a kappa distribution,” *Physics of Plasmas*, **30**, 4, 043903 (2023).
- [25] H. SUGIYAMA et al., “Electromagnetic ion cyclotron waves in the Earth’s magnetosphere with a kappa-Maxwellian particle distribution,” *Journal of Geophysical Research: Space Physics*, **120**, 10, 8426 (2015).
- [26] P. ASTFALK and F. JENKO, “LEOPARD: A grid-based dispersion relation solver for arbitrary gyrotrropic distributions,” *Journal of Geophysical Research: Space Physics*, **122**, 1, 89 (2017).
- [27] D. VERSCHAREN et al., “ALPS: the Arbitrary Linear Plasma Solver,” *Journal of Plasma Physics*, **84**, 4, 905840403 (2018).
- [28] K. G. KLEIN and D. VERSCHAREN, “The dielectric response of plasmas with arbitrary gyrotrropic velocity distributions,” *Physics of Plasmas*, **32**, 9, 092104 (2025).
- [29] H. XIE, “Efficient framework for solving plasma waves with arbitrary distributions,” *Physics of Plasmas*, **32**, 6, 060702 (2025).
- [30] T. H. STIX, *Waves in Plasmas*, American Institute of Physics, Melville, NY, 1 edition, (1992), Published: 01 December 1992.
- [31] D. SUMMERS and R. M. THORNE, “Plasma microinstabilities driven by loss-cone distributions,” *Journal of Plasma Physics*, **53**, 3, 293 (1995).
- [32] K. RONNMARK, “Computation of the dielectric tensor of a Maxwellian plasma,” *Plasma Physics*, **25**, 6, 699 (1983).
- [33] M. NAZEER, M. N. S. QURESHI, H. A. SHAH, and C. SHEN, “Effect of suprathermal particles on EMEC instability in kappa-Maxwellian distributed space plasmas,” *Astrophysics and Space Science*, **365**, 8, 140 (2020).

- [34] B. BASU and N. J. GROSSBARD, “Ion-cyclotron instability in current-carrying Lorentzian (kappa) and Maxwellian plasmas with anisotropic temperatures: A comparative study,” *Physics of Plasmas*, **18**, 9, 092106 (2011).

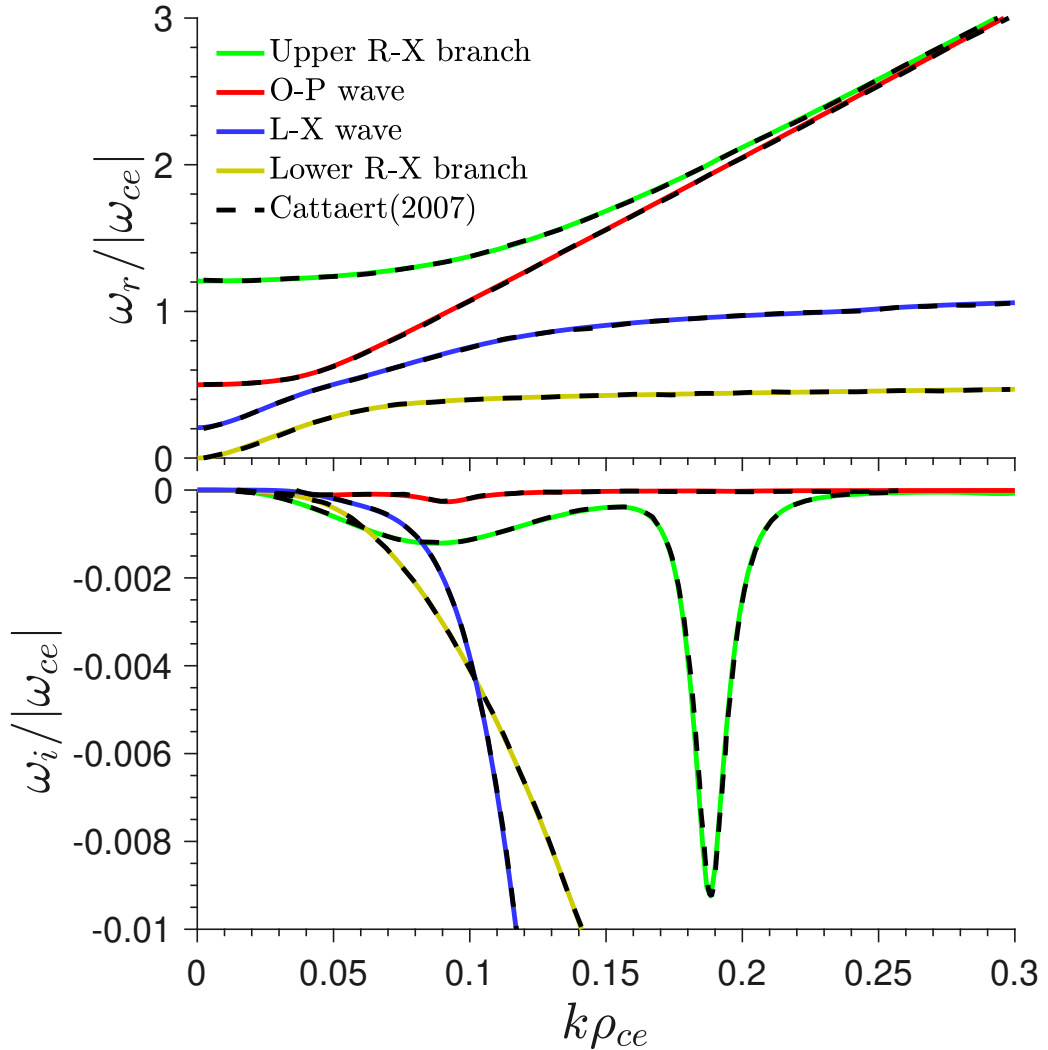


Figure 3: $\omega_r/|\omega_{ce}|$ vs. ρ_{ce} (top) and $\omega_i/|\omega_{ce}|$ vs. ρ_{ce} (bottom) for $\kappa_{\parallel e} = 1$, $\kappa_{\perp e} = 200$, $\theta = 30^\circ$, $\tilde{\theta}_{\perp e}/c = 0.1$, $\omega_{pe}/|\omega_{ce}| = 0.5$, $T_{\perp e}/T_{\parallel e} = 1$, and $B_0 = 1.0 \times 10^{-6}$ T, comparison with data from Fig. 1 of Cattaert et al. [13] (black dashed lines).

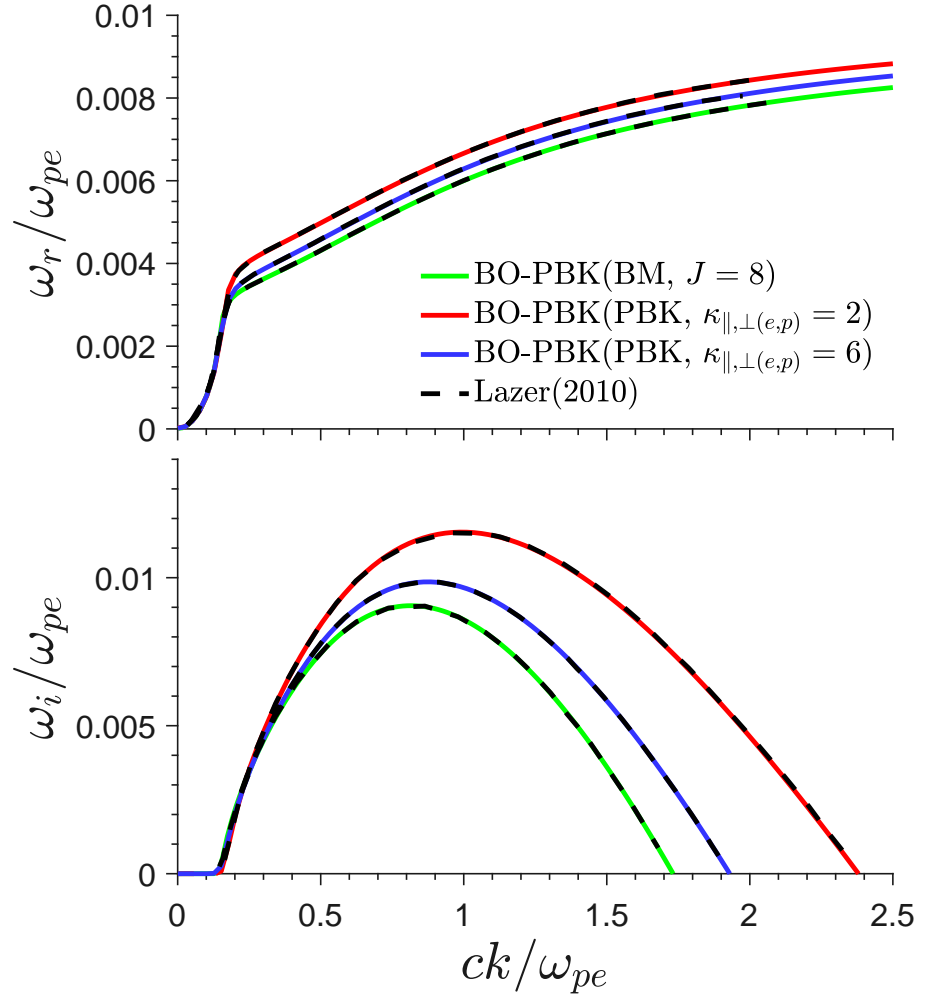


Figure 4: Comparison of real frequency ω_r (top) and growth rate ω_i (bottom) of parallel electron whistler-cyclotron modes for $\kappa_{\parallel,\perp(e,p)} = 2, 6, \infty$ in weakly magnetized plasmas ($|\omega_{ce}|/\omega_{pe} = 0.01$), with $v_{T\parallel e} = 0.02c$ and $T_{\perp(e,p)}/T_{\parallel(e,p)} = 4$. Data from Fig. 2 of Lazer et al. [1], are shown as black dashed lines.

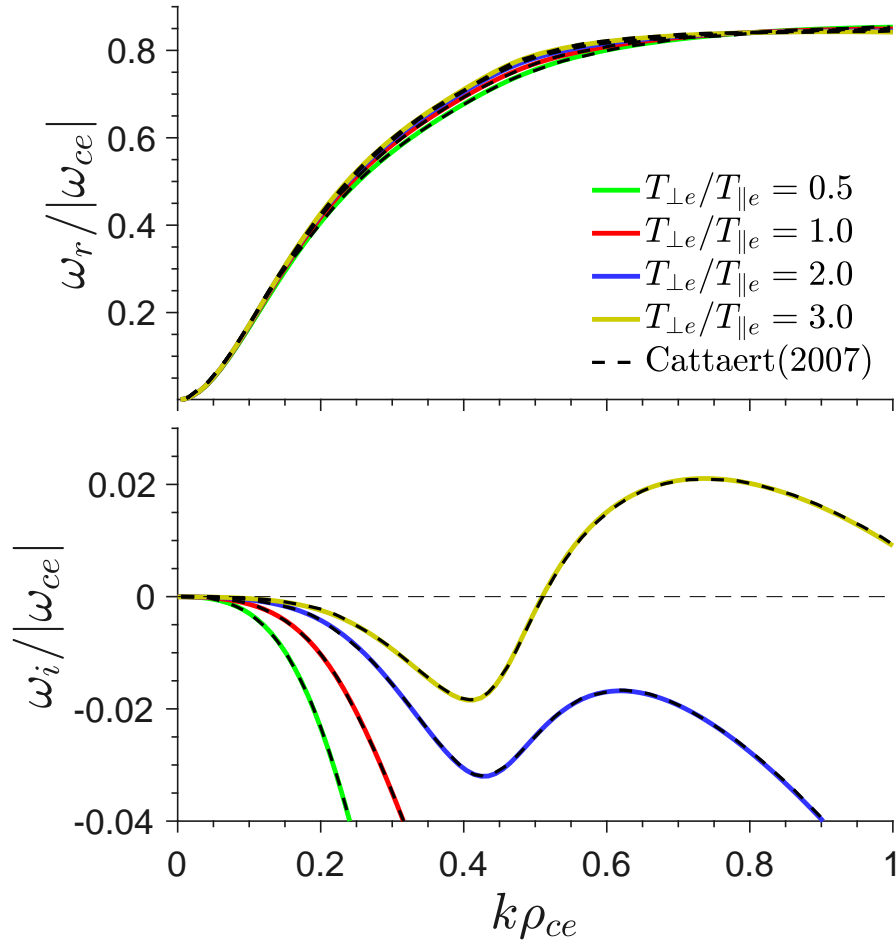


Figure 5: Comparison of whistler wave real frequency ω_r vs. k (top) and growth rate ω_i vs. k (bottom) with varying temperature anisotropy. Parameters: $\kappa_{\parallel e} = 1$, $\kappa_{\perp e} = 200$, $\theta = 30^\circ$, $\theta_{\perp e}/c = 0.1$, $|\omega_{ce}|/\omega_{pe} = 0.5$, and $B_0 = 1.0 \times 10^{-6}$ T. Comparison with data from Fig. 9 of Cattaert et al. [13] shown as dashed lines.

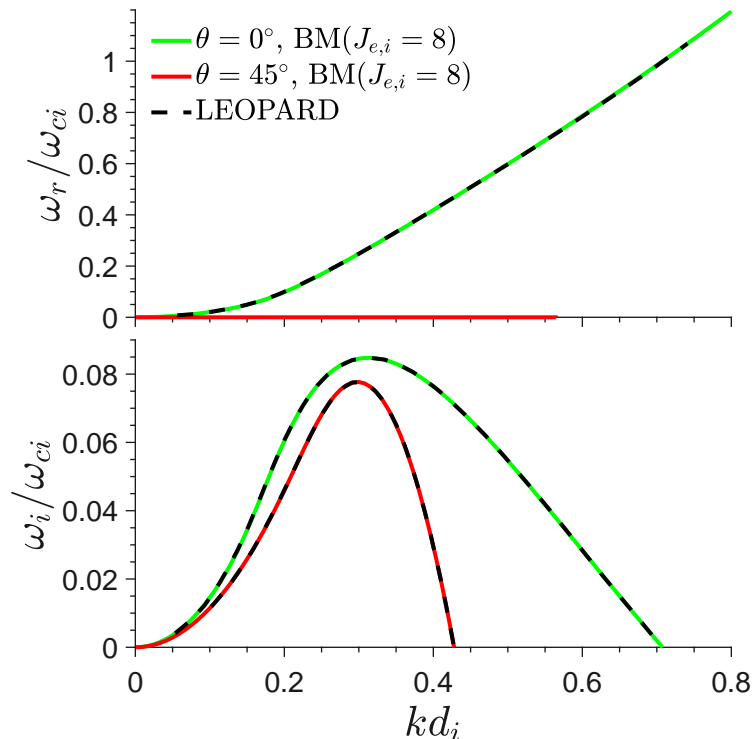


Figure 6: Benchmark of PFHI ($\theta = 0^\circ$) and OFHI ($\theta = 45^\circ$) for a BM distribution ($\beta_{\parallel i} = 4$, $\beta_{\perp i} = 2$, and $\beta_e = 1$). Top: real frequency ω_r ; bottom: growth rate ω_i . The black dashed lines represent the LEOPARD data from Fig. 1 in Ref. [26].

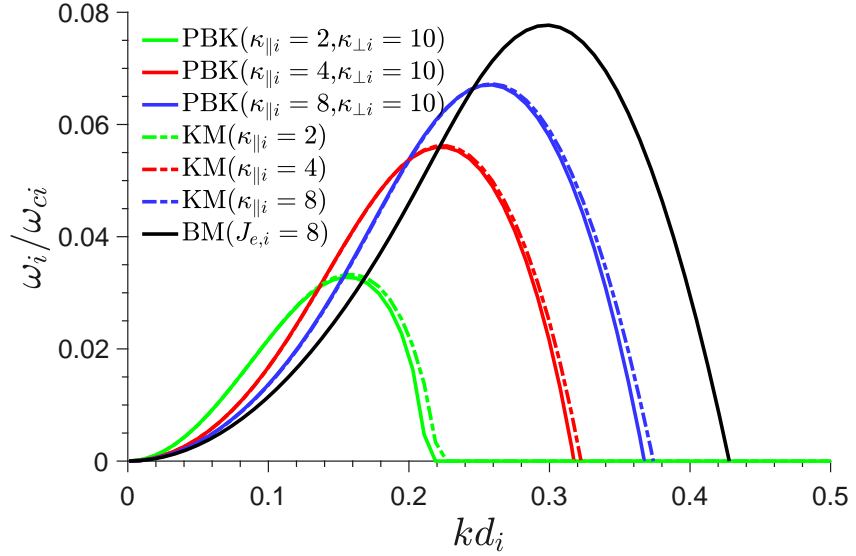


Figure 7: Comparison of OFHI ($\theta = 45^\circ$) for ion distributions: BM (black solid line), KM ($\kappa_{\parallel i} = 2, 4, 8$, $\kappa_{\perp i} = 200$, dashed green, red and blue lines) and PBK($\kappa_{\parallel i} = 2, 4, 8$, $\kappa_{\perp i} = 10$, solid green, red and blue lines).

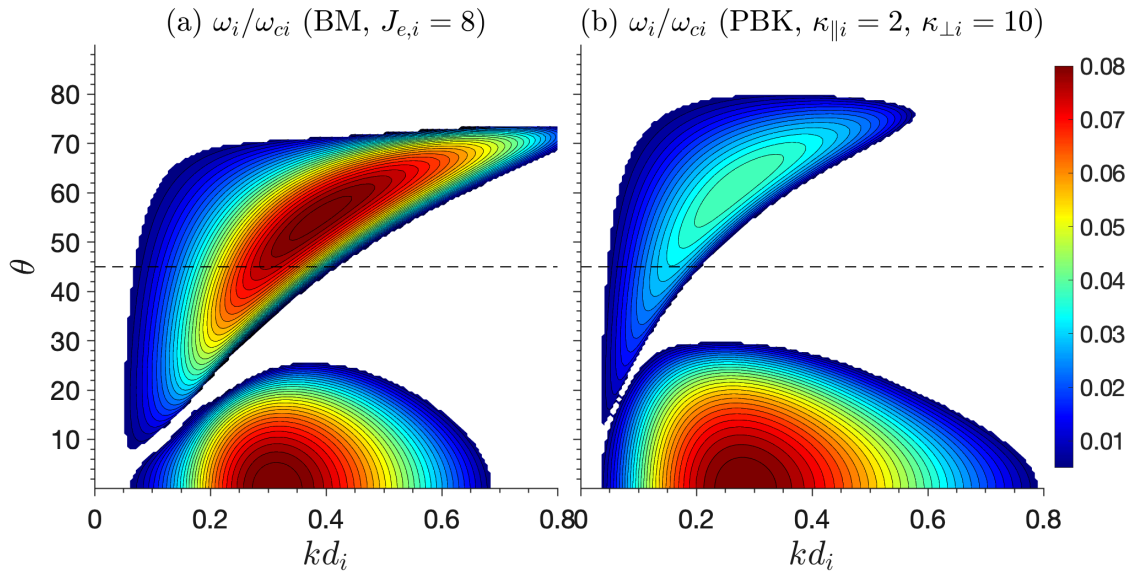


Figure 8: Comparison of the PFHI and OFHI for ions with (a) BM and (b) PBK distributions at various propagation angles.

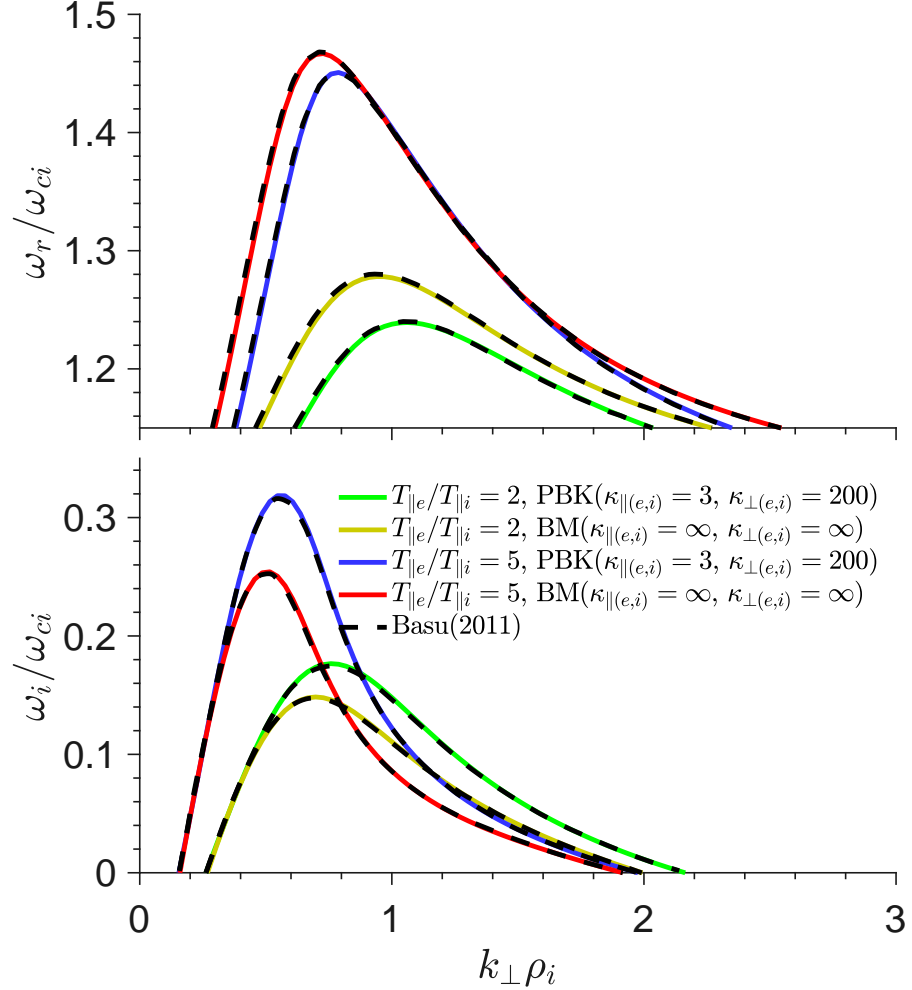


Figure 9: ω_r/ω_{ci} vs. $k_{\perp}\rho_i$ (top) and ω_i/ω_{ci} vs. $k_{\perp}\rho_i$ (bottom) for $\omega_{pe}/|\omega_{ce}| = 1/15$, $u_{e0}/(\tilde{\theta}_{\parallel e}/\sqrt{2}) = 1$, $k_{\parallel}/(\sqrt{2}\rho_i) = 0.08$, $T_{\parallel i}/T_{\perp i} = 1$, and $T_{\parallel e}/T_{\parallel i} = 2, 5$. Solid colored curves: results from the BO-PBK solver for PBK ($\kappa_{\parallel(e,i)} = 3$, $\kappa_{\perp(e,i)} = 200$) and BM ($\kappa_{\parallel(e,i)} = \infty$, $\kappa_{\perp(e,i)} = \infty$) plasmas. The black dashed lines are data from Fig. 6 of Basu et al. [34] for comparison.

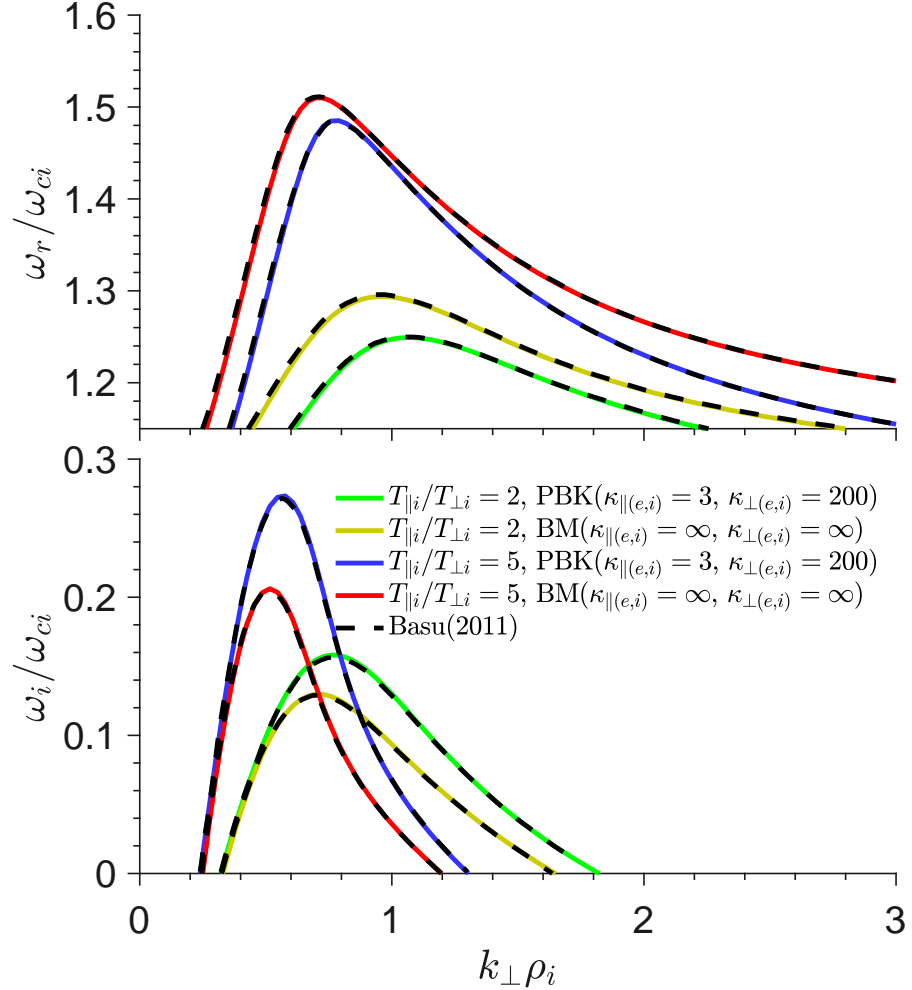


Figure 10: ω_r/ω_{ci} vs. $k_{\perp}\rho_i$ (top) and ω_i/ω_{ci} vs. $k_{\perp}\rho_i$ (bottom) for $\omega_{pe}/|\omega_{ce}| = 1/15$, $u_{e0}/(\tilde{\theta}_{\parallel e}/\sqrt{2}) = 1$, $k_{\parallel}/(\sqrt{2}\rho_i) = 0.08$, $T_{\parallel e}/T_{\parallel i} = 1$, and $T_{\parallel i}/T_{\perp i} = 2, 5$. Solid colored curves: results from BO-PBK solver for PBK ($\kappa_{\parallel(e,i)} = 3$, $\kappa_{\perp(e,i)} = 200$) and BM ($\kappa_{\parallel(e,i)} = \infty$, $\kappa_{\perp(e,i)} = \infty$) plasmas. The black dashed lines are data from Fig. 7 of Basu et al. [34] for comparison.

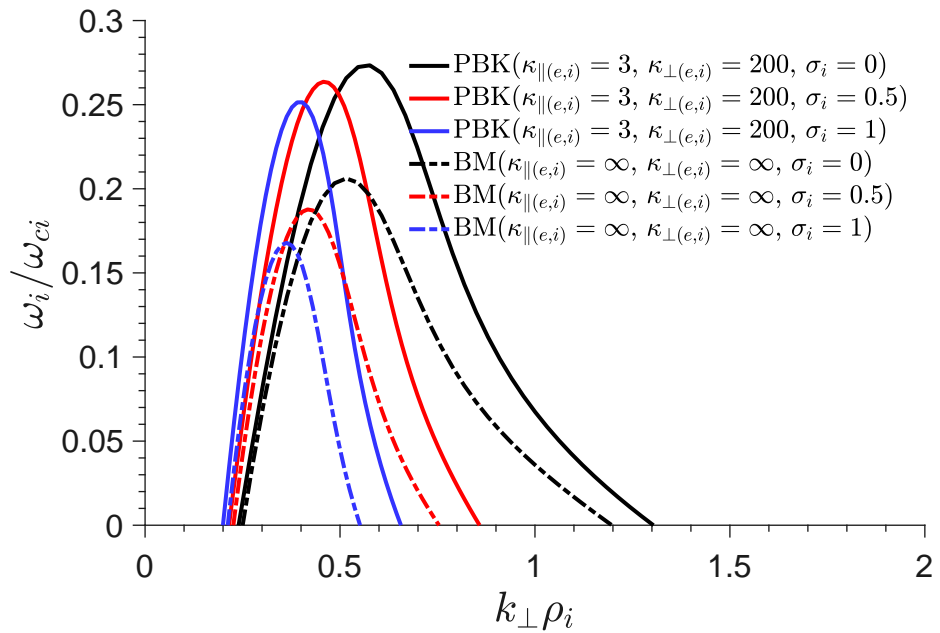


Figure 11: ω_i/ω_{ci} vs. $k_{\perp}\rho_i$ for parameters $\omega_{pe}/|\omega_{ce}| = 1/15$, $u_{e0}/(\tilde{\theta}_{\parallel e}/\sqrt{2}) = 1$, $k_{\parallel}/(\sqrt{2}\rho_i) = 0.08$, $T_{\parallel e}/T_{\parallel i} = 1$, and $T_{\parallel i}/T_{\perp i} = 5$. Solid curves show results for the PBK model ($\kappa_{\parallel(e,i)} = 3$, $\kappa_{\perp(e,i)} = 200$) and dashed curves for the BM model ($\kappa_{\parallel(e,i)} = \infty$, $\kappa_{\perp(e,i)} = \infty$) both for a loss-cone distribution with $\sigma_i = 0$ (black), 0.5 (red), and 1 (blue).

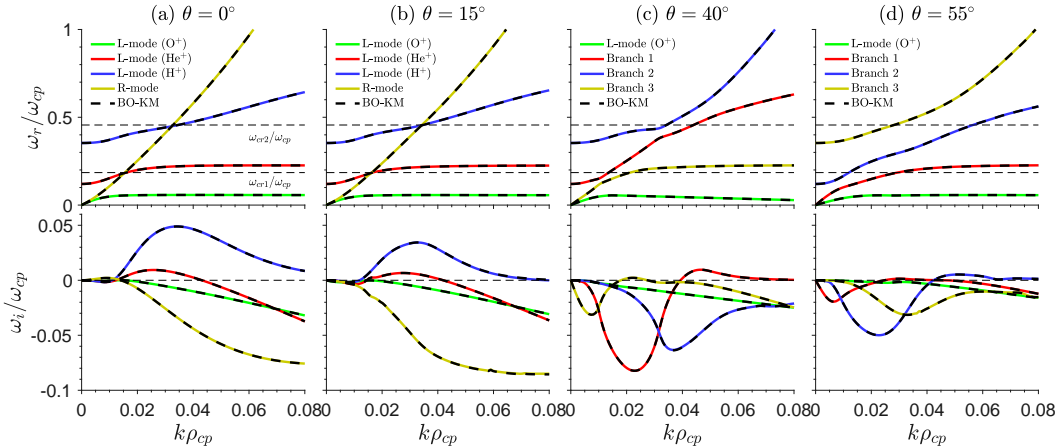


Figure 12: ω_r/ω_{cp} vs. $k\rho_{cp}$ (top) and ω_i/ω_{cp} vs. $k\rho_{cp}$ (bottom) for EMIC waves at propagation angles (a) $\theta = 0^\circ$, (b) 15° , (c) 40° , and (d) 55° . Solid colored curves show BO-PBK solver results, while black dashed lines indicate data from Fig. 13 of Bai et al. [15]. Lower and upper dashed lines in the top panels denote the first and second crossover frequencies, ω_{cr1}/ω_{cp} and ω_{cr2}/ω_{cp} .